Registration of 4D Cardiac CT Sequences Under Trajectory Constraints With Multichannel Diffeomorphic Demons

Jean-Marc Peyrat, Hervé Delingette*, Maxime Sermesant,
Chenyang Xu, *Senior Member, IEEE*, and Nicholas Ayache

***Abstract*—We propose a framework for the nonlinear spatiotemporal registration of 4D time-series of images based on the *Diffeomorphic Demons* (DD) algorithm. In this framework, the 4D spatiotemporal registration is decoupled into a 4D temporal registration, defined as mapping physiological states, and a 4D spatial registration, defined as mapping trajectories of physical points. Our contribution focuses more specifically on the 4D spatial registration that should be consistent over time as opposed to 3D registration that solely aims at mapping homologous points at a given time-point. First, we estimate in each sequence the motion displacement field, which is a dense representation of the point trajectories we want to register. Then, we perform simultaneously 3D registrations of corresponding time-points with the constraints to map the same physical points over time called the *trajectory constraints*. Under these constraints, we show that the 4D spatial registration can be formulated as a *multichannel registration* of 3D images. To solve it, we propose a novel version of the *Diffeomorphic Demons* (DD) algorithm extended to vector-valued 3D images, the *Multichannel Diffeomorphic Demons* (MDD). For evaluation, this framework is applied to the registration of 4D cardiac CT sequences and compared to other standard methods with real patient data and synthetic data simulated from a physiologically realistic electromechanical cardiac model. Results show that the trajectory constraints act as a temporal regularization consistent with motion whereas the multichannel registration acts as a spatial regularization. Finally, using these trajectory constraints with multichannel registration yields the best compromise between registration accuracy, temporal and spatial smoothness, and computation times. A prospective example of application is also presented with the spatiotemporal registration of 4D cardiac CT sequences of the same patient before and after radiofrequency ablation (RFA) in case of atrial fibrillation (AF). The intersequence spatial transformations over a cardiac cycle allow to analyze and quantify the regression of left ventricular hypertrophy and its impact on the cardiac function.**

***Index Terms*—Registration, 4D, Sequence, Spatiotemporal, Cardiac, Heart, CT, Multichannel, Trajectory Constraints.**

Manuscript received September 24, 2009; revised November 23, 2009. This work was supported by INRIA (Sophia Antipolis, France), Siemens Corporate Research (Princeton, NJ, USA) and Microsoft Research (Cambridge, UK). *Asterisk indicates corresponding author.*

J.-M. Peyrat, H. Delingette and N. Ayache are with the INRIA, Asclepios Research Project, 2004, route des Lucioles, BP 93, 06902 Sophia Antipolis Cedex, France (*corresponding author - email: herve.delingette@inria.fr).

M. Sermesant is with the INRIA, Asclepios Research Project, Sophia Antipolis, France, and with King's College London, School of Medicine, Division of Imaging Sciences, St Thomas Hospital, SE1 7EH, London, UK.

C. Xu is with Siemens Corporate Research, Department of Imaging and Visualization, Princeton, NJ 08540 USA.

I. Introduction

DURING the last decade, the improvement of medical imaging technologies extended 3D image acquisitions to 4D sequence acquisitions such as cine MRI, tagged MRI, 4D CT or 4D ultrasound. They give access to additional information important for studying the motion of organs (such as heart and lung) or for real-time control during image-guided surgical procedures. Since the temporal dimension cannot be considered as an additional spatial dimension, the extension of 3D image processing tools to 4D spatiotemporal data is not straightforward. Thus, the development of specific algorithms for spatiotemporal data is necessary such as temporal interpolation [1], segmentation [2]–[11], statistical analysis of cardiac shape and dynamics [12], [13], motion tracking [14]–[26], image-to-sequence registration [27], [28], temporal alignment [29], [30], and spatiotemporal registration [30]–[35]. Most of the spatiotemporal registration algorithms deal with the registration of sequences of the same patient acquired with different imaging modalities. Recently, research has addressed the more complex intersubject spatiotemporal registration of sequences. Some 3D image registration applications were extended to 4D sequences, such as registration-based segmentation [34] or atlas construction [12]. Furthermore, it opens doors to applications specific to spatiotemporal data, for instance by comparing the temporal evolution of local parameters of homologous anatomical points (such as strain or depolarization/repolarization times) or by analyzing the temporal change of intersequence transformations over a cardiac cycle to better understand anatomical and functional differences.

Caspi and Irani [31] were among the first to propose a framework for sequence-to-sequence alignment using spatiotemporal transformations. Since their algorithm was designed for the registration of different camera views of the same dynamic scene, they constrained the spatiotemporal transformation to a 1D temporal linear transformation to cope with the different acquisition rates of the cameras and to a 3D affine transformation constant over time to cope with the different camera views. They showed that folding spatial and temporal information into a single alignment framework outperforms a purely image-to-image alignment of corresponding frames.

Sundar *et al.* [23] proposed to embed cardiac motion tracking into a 4D registration framework. The original sequence is registered to a static sequence built from the image at a ref-

erence time-point. All 3D transformations from a given time-point to the reference time-point are determined simultaneously with spatiotemporal smoothness constraints. Compared to the independent 3D registration of each time-point to the reference time-point, this method showed more robust results. But since this framework was limited to motion estimation in a single sequence, issues specific to the comparison of different sequences, like temporal misalignment and large intersequence deformations, were not addressed.

Perperidis *et al.* [30] proposed to register two cardiac MR sequences of different patients with spatiotemporal free-form deformation models based on B-Splines. The registration algorithm optimizes either the spatial and temporal transformation models simultaneously or optimizes the temporal transformation before optimizing the spatial transformation. The temporal transformation is a 1D B-Spline transformation that corrects temporal misalignment caused by length differences of the cardiac cycles and by kinetic differences of cardiac phases. The spatial transformation is a single 3D B-Spline transformation that corrects spatial misalignment at all corresponding time-points caused by global anatomical differences. Since the same intersubject spatial transformation is used over time, residual anatomical differences occur between corresponding time-points. These differences are used to build a probabilistic MR cardiac atlas representing the anatomy and function of a healthy heart.

To catch those residual differences and to fully map corresponding images at each time-point, a time-dependent spatial transformation is necessary. When registering 4D lung CT sequences of the same patient for image-guided radiotherapy, Schreibmann *et al.* [35] determined a spatial 3D B-Spline transformation independently at selected time-points. For intersubject registration of cardiac cine MRIs where the anatomies and motion patterns can have high discrepancies between patients, Lopez *et al.* [34] extended this solution by including image information from neighboring time-points (called bridging points). They computed a 3D B-Spline transformation at each time-point with an energy functional matching simultaneously the normalized mutual information of three pairs of images: the pair of images at the current time-point and two pairs of images at the neighboring time-points transformed to the geometry of the current time-point with intrasubject motion transformations. Their results show an improvement of the registration accuracy by comparing endocardial and atrial segmentations. But in both methods, the 3D B-Spline transformations are computed independently at each time-point. Thus they are not necessarily consistent with motion occurring in each sequence by matching the same physical points at different time-points. This constraint is important when comparing the temporal evolution of local parameters of homologous anatomical points.

In this article, we propose a framework in which the resulting intersequence spatial transformations verify the constraints to map the same physical points over time, called the *trajectory constraints*. In this framework, the 4D spatiotemporal registration is decoupled into a 4D temporal registration, defined as mapping physiological states, and a 4D spatial registration, defined as mapping trajectories of physical points. A temporal registration is performed using global cardiac physiological state parameters. We first perform the 4D temporal registration based on the electrocardiogram (ECG) that define a global cardiac electrophysiological state as a percentage of the R-R interval (interval between two consecutive R peaks of the ECG). It provides a linear temporal transformation that ensures to match the beginning and the end of cardiac cycles, which is the end of diastole (ED). This linear transformation is then refined by temporally aligning the blood volume curves with a nonlinear transformation matching global mechanical states such as the end of systole (ES). After this global temporal alignment, we perform a 4D spatial registration. Our contribution focuses more specifically on the improvement of this 4D spatial registration step by enforcing the trajectory constraints. A motion tracking is performed with the *Diffeomorphic Demons* (DD) algorithm [36] to determine the dense trajectories of points in both sequences. These dense trajectories in the two sequences are used to constrain temporally the intersequence spatial transformations. Including the trajectory constraints, we show that the 4D spatial registration can be formulated as a *multichannel registration* of 3D images at a reference time point combined with inversions and compositions of transformations. We also present a novel version of the multichannel 3D registration algorithm based on the DD, the *Multichannel Diffeomorphic Demons* (MDD). A preliminary study of this framework has already been published in [37]. This framework is applied to the intersubject registration of 4D cardiac CT sequences and compared to other standard methods with real patient data and synthetic data simulated from a physiologically realistic electromechanical cardiac model [38]. The validation of registration algorithms is not an easy task, especially in the context of intersubject registration where ground truth transformations are not known, and even more difficult when dealing with sequences of images. Thus, we evaluated the registration results of real data with LV/RV endocardial and epicardial segmentations that gives the opportunity to quantify the quality of the myocardium registration. Results show that using the trajectory constraints yields a temporal regularization consistent with motion whereas using the multichannel registration yields a better spatial regularization. The combination of these two showed to be the best compromise between registration accuracy, temporal consistency with motion tracking, spatial smoothness, and computation times. We end this article by presenting a possible application of 4D spatiotemporal registration with pre- and post-operative data where intersequence transformations over time could be used to study and quantify the coupling between anatomical and functional remodeling.

II. Spatiotemporal Registration Setting

In this section, we describe the general setting for the spatiotemporal registration of 4D sequences that estimates two different types of intersequence transformations: a temporal transformation and a spatial transformation. First, we introduce the temporal transformation as a physiological state mapping. Second, we present the 4D spatial registration as a trajectory mapping from which we derive a discrete formulation of the trajectory constraints that should be verified.

A. General Setting

Let's consider the reference sequence I and the target sequence I' whose acquisition space-time are respectively $\Omega \times \tau \subset \mathbb{R}^3 \times \mathbb{R}$ and $\Omega' \times \tau' \subset \mathbb{R}^3 \times \mathbb{R}$:

$$\begin{array}{rccl} I': & \Omega' \times \tau' & \longrightarrow & \mathbb{R} \\ & (x', t') & \longmapsto & I'(x', t') = i' \end{array}$$

$$\begin{array}{rccl} I: & \Omega \times \tau & \longrightarrow & \mathbb{R} \\ & (x, t) & \longmapsto & I(x, t) = i \end{array}$$

When registering the target sequence I' to the reference sequence I, the spatiotemporal transformation S that maps a spatiotemporal position (x, t) of I to the corresponding spatiotemporal position (x', t') of I' must be found:

$$\begin{array}{rccl} S: & \Omega \times \tau & \longrightarrow & \Omega' \times \tau' \\ & (x, t) & \longmapsto & S(x, t) = (x', t') \end{array}$$

The spatiotemporal transformation S can be formulated as the combination of a spatial transformation S_{space} and a temporal transformation S_{time} as follows:

$$S(x, t) = (S_{\text{space}}(x, t), S_{\text{time}}(x, t))$$

In the following, we get more into details of these two types of transformation where the temporal transformation maps corresponding physiological states and the spatial transformation maps corresponding trajectories of physical points.

B. Temporal Transformation as Physiological State Mapping

The temporal transformation S_{time} is defined as follows:

$$\begin{array}{rccl} S_{\text{time}}: & \Omega \times \tau & \longrightarrow & \tau' \\ & (x, t) & \longmapsto & S_{\text{time}}(x, t) = t' \end{array}$$

The idea behind the temporal transformation is to match an event occurring at the time-point t and the spatial position x in the reference sequence to a similar event occurring at the corresponding time-point t' in the target sequence. In medical imaging, corresponding time-points can be defined as time-points at which physiological states are the same, for instance the end of diastole/systole for a given cardiac ventricle or the beginning of a respiration cycle for a lung. Thus the temporal transformation is highly dependent on which physiological parameters we want to compare. Examples of possible global physiological parameters are shown in Fig. 1. In previous works, the temporal transformation S_{time} was determined by matching a parameter describing a global physiological state of the heart such as a specific event of the ECG (e.g. P, Q, R, S, and T peaks), volume extrema of the left ventricle, the average cross-correlation coefficient between frame intensities [30], [39] or the path of a specific anatomical point [29]. Since these global parameters are the same for every position at a given time-point, the resulting temporal transformation is independent of the spatial position x and thus a function of time only. Actually the temporal transformation can be space dependent when two structures have different physiological patterns. For instance the periods of the cardiac and respiration cycles are different and the temporal transformation of a sequence imaging heart and lungs should be different for each organ. It could also happen with different areas of a single organ. For instance we might want to temporally register independently the left and right cardiac ventricles in pathological cases such as a left bundle branch block (LBBB) where the activation of the left ventricle is delayed, which results in the left ventricle contracting later than the right ventricle. We could also imagine to temporally register events that are locally defined such as depolarization/repolarization or maximum contraction that are spatially dependent. Obviously the temporal transformation can become very complex when comparing local physiological events. The complexity of the temporal transformation and the choice of the features used for temporal registration should be governed by the desired application.

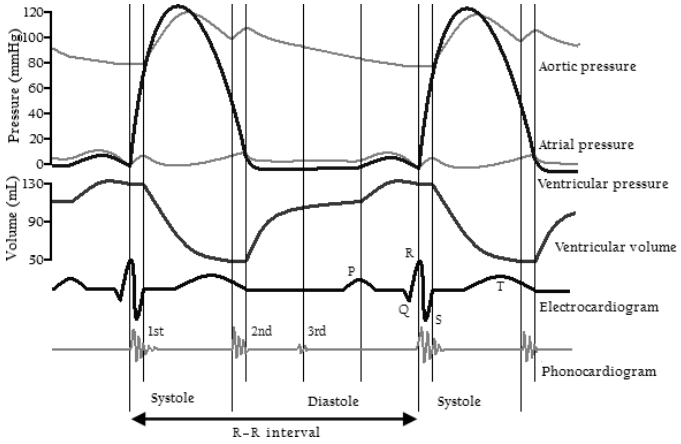

Fig. 1. Wiggers Diagram [40] - This diagram shows different physiological parameters with the same time-line of a cardiac cycle: pressure and volume curves, ECG, and phonocardiogram (figure adapted from Wikipedia - http://en.wikipedia.org/wiki/Cardiac_cycle). These physiological parameters can be used to detect different physiological events occurring in a cardiac cycle such as diastole, systole, or valves opening and closing.

As mentioned previously, the temporal transformation is determined by the registration of some signals or quantities that may not be intensity-based (cf. Fig. 1) whereas the spatial registration is intensity-based. Thus, when using different data, the temporal transformation S_{time} can be determined independently from the spatial transformation S_{space}. The temporal transformation can even be applied after the spatial transformation as long as structures are not appearing and/or disappearing during the sequences and as long as images at each time-point in the reference sequence has an image at the same time point in the target sequence to be compared to. This happens when the same structures are present during the whole sequence and when the acquisition time intervals τ and τ' exactly overlap, which is the case after global linear temporal registration. This linear transformation is often implicitly performed in the acquisition process such as in 4D cardiac CT sequences that are gated from the end of diastole (ED) of a cardiac cycle to the ED of the next cycle.

In our following experiments registering 4D cardiac CT sequences, we first define the global physiological state with the ECG (R-R interval in Fig. 1) temporally aligned with a linear transformation. In practice, this linear transformation

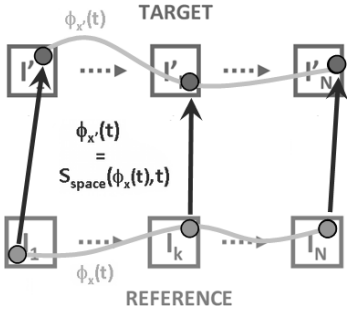

Fig. 2. Trajectory-based registration - Spatial transformations should map corresponding physical points X and X' lying on the same trajectory (respectively $\phi_X(t)$ and $\phi_{X'}(t)$) at different time points.

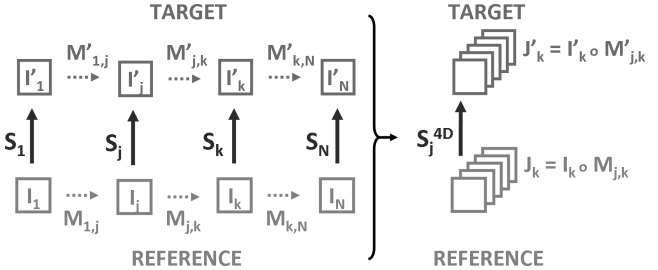

(a) 4D Registration (b) Multichannel 3D Registration

Fig. 3. (a) Discretization of the 4D spatial registration with the spatial transformations S_j between the sequences at time t_j and the motion transformations $M_{j,k}$ and $M'_{j,k}$ between frames at times t_j and t_k (note that the arrows show the direction of the resampling deformation fields used to transform the target image to the reference image) - (b) Under trajectory constraints, the 4D registration can be parametrized by a single reference spatial transformation S_j^{4D} and thus formulated as a multichannel 3D registration problem. Frames I_k and I'_k of the two sequences are transformed through the motion transformations $M_{j,k}$ and $M'_{j,k}$ to the reference geometry of images I_j and I'_j. The transformations S_k^{4D} are then reconstructed from S_j^{4D} to satisfy the trajectory constraint: $S_k^{4D} = M'_{j,k} \circ S_j^{4D} \circ M_{j,k}^{-1}$.

is implicitly performed in the ECG-gated acquisition process of 4D cardiac CT where each frame correspond to a percentage of the R-R interval. Then, a nonlinear temporal transformation refines the linear transformation by matching global mechanical state defined with blood volume curves. In this way, the following intersequence spatial registration between corresponding frames are performed at corresponding mechanical states and thus with similar geometries.

When the temporal transformation is known, sequences can be temporally resampled. Due to the nature of the temporal dimension, one should note that the temporal interpolation cannot be performed only as an intensity-based linear interpolation of images without coping with the motion occurring in the sequence. Temporal interpolation should rely on a motion-based interpolation of images as proposed by Ehrhardt *et al.* [1]. Thus motion tracking, computed as described in the following Section III, is necessary for the temporal resampling of sequences.

C. Spatial Transformation as Trajectory Mapping

The spatial transformation S_{space} is defined as follows:

$$\begin{array}{rccl} S_{\text{space}}: & \Omega \times \tau & \longrightarrow & \Omega' \\ & (x,t) & \longmapsto & S_{\text{space}}(x,t) = x' \end{array}$$

To be physically meaningful when determining the time-dependent spatial transformation S_{space}, the same physical points should be mapped at different time points in both sequences as shown in Fig. 2. In other words, if we define the position of a physical point X over time as the trajectory ϕ_X:

$$\begin{array}{rccl} \phi_X: & \tau & \longrightarrow & \Omega \\ & t & \longmapsto & \phi_X(t) = x \end{array}$$

we can formulate the problem as finding the transformation S_{space} such that the trajectory ϕ_X of a physical point X in the reference sequence maps the trajectory $\phi_{X'}$ of its corresponding physical point X' in the target sequence:

$$S_{\text{space}}\left(\phi_X(\cdot),\cdot\right) = \phi_{X'}(\cdot) \tag{1}$$

With this formulation we can easily understand why matching corresponding trajectories is independent from matching corresponding time-points as mentioned in the previous section. Indeed a temporal transformation does not modify the nature of a trajectory but does solely modify the speed of a physical point along its trajectory. It simply means that a temporal transformation does not modify the anatomical position of a physical point but does only modify its physiological state over time. Our goal here is to provide a robust intensity-based image matching of corresponding anatomical points when temporal alignment of sequences has already been performed by matching corresponding physiological events as proposed in previous Section II-B.

The temporal discretization of the 4D spatial registration is illustrated in Fig. 3 (note that we call transformations the resampling transformations used to deform the target image to the reference image, the arrows show the direction of the resampling deformation fields used to find the corresponding point of the reference image in the target image). The intersequence transformations S_j map the reference volume I_j to the target volume I'_j at time t_j knowing the trajectories of points given by the intrasequence motion transformations $M_{j,j+1}$ and $M'_{j,j+1}$ between the times t_j and t_{j+1} respectively in the reference and target sequences. In the discrete world, Equation 1 is equivalent to stating that if a point position x in image I_j maps a point position x' in I'_j by the intersequence transformation S_j then the remaining intersequence transformations S_{j+1} should map the displaced point position $M_{j,j+1}(x)$ to the displaced point position $M'_{j,j+1}(x')$. This translates into a set of constraints, called the trajectory constraints, that link the intersequence transformations S_j and S_k with the motion transformations $M_{j,k}$ (from I_j to I_k) and $M'_{j,k}$ (from I'_j to I'_k) :

$$S_k \circ M_{j,k} = M'_{j,k} \circ S_j \tag{2}$$

In the sequel, we formulate the 4D spatial registration as the minimization of a functional including those trajectory constraints and considering the motion tracking as a known parameter previously computed independently in each sequence.

III. From 4D Registration to Multichannel 3D Registration

When determining the intersequence transformation S_j, the standard approach is to minimize the image similarity measure between the pair of images (I_j, I'_j) :

$$S_j^{3D} = \underset{S}{\operatorname{argmin}} \left(\int_{\omega \in \Omega_j} \text{Sim}(\ I_j(\omega),\ I'_j \circ S(\omega)\ )\ d\omega \right) \quad (3)$$

We call this intersequence transformation S_j^{3D} the solution to the 3D registration problem that only involves one pair of images (I_j, I'_j).

When determining the set of intersequence transformations $(S_j^{4D})_{j=1,...,N}$ for the 4D spatial registration, we want to simultaneously minimize the image similarity measure between all pairs of images (I_j, I'_j) :

$$(S_1^{4D}, ..., S_N^{4D}) = \underset{(S_1,...,S_N)}{\operatorname{argmin}} \left(\sum_{k=1}^{N} \int_{\omega \in \Omega_k} \text{Sim}(\ I_k(\omega),\ I'_k \circ S_k(\omega)\ )\ d\omega \right) \quad (4)$$

If each transformation S_j^{4D} is considered independent from the others, the solution is similar to finding each transformation S_j^{3D}. Actually to ensure that the transformations $(S_j^{4D})_{j=1,...,N}$ map the same physical point over time, the trajectory constraints of Equation 2 should be verified. Thus a strong link exists between all intersequence transformations that cannot be considered independent anymore. The trajectory constraints can be reformulated as $S_k^{4D} = M'_{j,k} \circ S_j^{4D} \circ M_{j,k}^{-1}$ that may be interpreted as follows: to satisfy the trajectory constraints, the transformation $M'_{j,k} \circ S_j^{4D} \circ M_{j,k}^{-1}$ should map image I_k into image I'_k.

Motion tracking is performed with an updated Lagrangian scheme with Gaussian regularization. Basically, the intrasequence motion transformations $M_{j,k}$ and $M'_{j,k}$ are iteratively computed by initializing the registration of frame t_k to reference frame t_j in each sequence with the motion transformations $M_{j,k-1}$ and $M'_{j,k-1}$ obtained at the previous step. Since motion tracking is necessary to temporally resample the sequences when using motion-based interpolation, motion tracking is actually performed with the original sequences before temporal resampling. Then motion tracking is also temporally resampled according to the temporal transformation in order to be consistent with the temporally resampled sequence.

In the remainder, we consider the motion transformations $M_{j,k}$ and $M'_{j,k}$ as fixed when determining the intersequence transformation S_j^{4D}. Indeed, motion tracking is intrinsically independent from any intersequence registration. Motion transformations are estimated independently and then used to improve the estimation of the intersequence transformations. This assumption makes sense when considering that the motion transformations are much easier to estimate than intersequence transformations. Indeed, intersequence transformations have larger deformations than motion transformations (especially in sequences with high temporal resolution). Furthermore, they are less constrained than cardiac motion, since cardiac motion follows the law of biomechanics that can be included as an *a priori* knowledge, for instance elasticity or near incompressibility of cardiac tissue [24], [41]. In this way, physically meaningful constraints on the estimation of the intrasequence motion transformations would be indirectly included to the estimation of intersequence anatomical transformations through the trajectory constraints.

Applying the trajectory constraints to the set of variables $(S_j)_{j=1,...,N}$ in the minimization process, any transformation S_k can be parametrized with a single transformation S_j at a reference time-point t_j and the motion transformations $M'_{j,k}$ and $M_{j,k}$. The number of unknown variables is highly decreased by determining only the chosen reference transformation S_j^{4D} that minimizes the following modified functional of Equation 4 :

$$S_j^{4D} = \underset{S}{\operatorname{argmin}} \left(\int_{\omega \in \Omega_j} \text{Sim}(\ I_j(\omega),\ I'_j \circ S(\omega)\ )\ d\omega + \sum_{k \neq j} \int_{\omega \in \Omega_k} \text{Sim}(\ I_k(\omega),\ I'_k \circ M'_{j,k} \circ S \circ M_{j,k}^{-1}(\omega)\ )\ d\omega \right) \quad (5)$$

Applying the appropriate change of variable $\omega = M_{j,k}(\nu)$ for each term of the functional, the 4D spatial registration can be formulated as the minimization of similarity criterion between several pairs of images:

$$S_j^{4D} = \underset{S}{\operatorname{argmin}} \left(\int_{\omega \in \Omega_j} \text{Sim}(\ I_j(\omega),\ I'_j \circ S(\omega)\ )\ d\omega + \sum_{k \neq j} \int_{\nu \in \Gamma_j} \text{Sim}(\ J_{j,k}(\nu),\ J'_{j,k} \circ S(\nu)\ )|\text{Jac}(M_{j,k})(\nu)|\ d\nu \right)$$

where $J_{j,k} = I_j \circ M_{j,k}$ and $J'_{j,k} = I'_j \circ M'_{j,k}$ are respectively the images at frame k transformed into the geometry of the image at frame j in the reference and target sequences, $\Gamma_j \in \Omega_j$ is part of image I_j, and $\text{Jac}(M_{j,k})$ is the Jacobian of transformation $M_{j,k}$.

In other words, the intersequence transformation S_j^{4D} must optimize the sum of similarity criteria between the pair of images (I_j, I'_j) and all pairs of images $(J_{j,k}, J'_{j,k})$ as shown in Fig. 3. Note also that the terms $\text{Jac}(M_{j,k})$ deriving from the change of variables take into account volume change of voxels when transforming I_k into $J_{j,k}$. This term acts as a voxel-wise weight map in each similarity criterion to ensure the equivalence of the energy functional formulated in the original and warped spaces. Once S_j^{4D} is estimated, the other transformations S_k^{4D} can be computed from S_j^{4D} with the trajectory constraints: $S_k^{4D} = M'_{j,k} \circ S_j^{4D} \circ M_{j,k}^{-1}$.

Finally, we have shown that including the trajectory constraints in the estimation of the intersequence transformation S_j^{4D} translates the 4D spatial registration problem into a single 3D multichannel registration problem associated with pairs of images (I_k, I'_k) transformed respectively in the reference space of the images I_j and I'_j.

The 4D spatiotemporal registration framework can be summarized as follows:

4D Spatiotemporal Registration Algorithm

(1) Temporal alignment w.r.t. global physiological parameters.
(2) Compute motion tracking $M_{j,k}$ and $M'_{j,k}$ registering each frame t_k to reference frame t_j.
(3) Resample motion tracking $M'_{j,k}$ and target sequence I' with motion-based interpolation.
(4) Transform each frame of I and I' to the reference frame with resampled $M_{j,k}$ and $M'_{j,k}$.
(5) Compute S_j^{4D} in the reference frame using 3D multichannel registration algorithm (cf. IV-B).
(6) Compute S_k^{4D} in other frames using the trajectory constraints : $S_k^{4D} = M'_{j,k} \circ S_j^{4D} \circ M_{j,k}^{-1}$.

IV. Multichannel 3D Diffeomorphic Demons

In this section, we present a novel extension of the *Diffeomorphic Demons* (DD) [36] to multichannel data (or vector-valued data). We have chosen to extend the DD algorithm but this choice is not exclusive. Other registration algorithms could also be extended to multichannel data. Due to the trajectory constraints, the space of resulting transformations should be stable by composition and inversion which is the case with DD. Mainly the speed of DD algorithm is a significant advantage when processing large 4D datasets in a reasonable amount of time. Recently, it has been shown in a thorough comparison of registration algorithms for brain applications [42] that DD was one of the fastest diffeomorphic registration algorithm [43]–[48].

We begin with the presentation of the diffeomorphic extension [36] of Thirion's Demons registration algorithm [49] for 3D images that is used to determine the motion transformations $M_{j,k}$ and $M'_{j,k}$. Then we present a novel extension of Demons algorithm to vector-valued images that is used to determine the reference intersequence transformation S_j^{4D} of the 4D registration framework.

A. Standard 3D Diffeomorphic Demons

The original Demons registration algorithm [49] is based on optical flow. But it has been shown that introducing a hidden variable, called the correspondences, the Demons can be formulated as a well-posed energy minimization with an alternate optimization scheme [50]. When registering the target 3D image I' to the reference 3D image I, the update transformation u of the current transformation S is first determined by minimizing the correspondences energy E^{corr} (cf. Equation 6) to obtain the correspondences transformation $c = S \circ u$. Second, the correspondences transformation c is regularized to obtain the new transformation S. The linearization of correspondences energy E^{corr} is formulated as follows:

$$E^{\text{corr}}(\mathbf{u}) \simeq \frac{1}{2|\Omega|} \int_{\omega \in \Omega} \left\| \begin{bmatrix} I(\omega) - I' \circ S(\omega) \\ \mathbf{0} \end{bmatrix} + \begin{bmatrix} \mathbf{G}^T(\omega) \\ \sigma(\omega)/\sigma_c \ \text{Id} \end{bmatrix} \mathbf{u}(\omega) \right\|^2 d\omega \quad (6)$$

where Ω is the overlap between I and $I' \circ S$, ω is the voxel position, $\mathbf{G}(\omega) = \frac{1}{2}(\nabla I(\omega) + \nabla I' \circ S(\omega))$ is the spatial gradient of intensity whose formulation comes from a linearization of the ESM scheme detailed in [36], $\sigma(\omega) = |I(\omega) - I' \circ S(\omega)|$ is the local estimation of the image noise, and σ_c is a fixed parameter that bounds the spatial uncertainty on the correspondences transformation. Note that the transformation u, which outputs a position, and its corresponding deformation field $\mathbf{u}$ are differentiated by bold characters. The link between them can be formulated as follows: $u = \text{Id} + \mathbf{u}$ where Id is the identity transformation.

A closed form solution of the minimization of the correspondences energy is given by the update vector field $\mathbf{u}$:

$$\mathbf{u} = -\frac{I - I' \circ S}{\mathbf{G}^T\mathbf{G} + \sigma^2/\sigma_c^2} \mathbf{G} \quad (7)$$

To constrain the update transformation to be diffeomorphic, the minimization of the functional is performed directly in the one-parameter subgroup of diffeomorphisms with stationary speed vector fields. Vercauteren *et al.* [36] showed that at a first order approximation this is equivalent to using the standard Demons algorithm and taking the exponential of the update transformation u. In this way, the update vector field $\mathbf{u}$ is the speed vector field parametrizing the update diffeomorphic transformation $v = \exp(u)$. The algorithm can be summarized as follows :

3D Diffeomorphic Demons Registration Algorithm (from [36])

(**A**) Choose an initial spatial transformation S.
(**B**) Iterate until convergence:
(B.1) Given S, compute the update vector field $\mathbf{u}$ with Equation 7.
(B.2) If a fluid-like regularization is used (typically a Gaussian kernel), let $\mathbf{u} \leftarrow K_{\text{fluid}} \star \mathbf{u}$.
(B.3) Fast computation of the exponential $\exp(u)$:
  (a) Choose n such that $\|2^{-n}\mathbf{u}\|$ is close enough to 0 (e.g. $\max\|2^{-n}\mathbf{u}(x)\| \leq 0.5$ voxel).
  (b) Perform an explicit first order integration: $\mathbf{v}(x) \leftarrow 2^{-n}\mathbf{u}(x)$ for all voxels x.
  (c) Do n (not 2^n!) recursive squarings of $v = \text{Id} + \mathbf{v}$: $v \leftarrow v \circ v$.
(B.4) Let $S \leftarrow S \circ v$.
(B.5) If a diffusion-like regularization is used (typically a Gaussian kernel), let $\mathbf{S} \leftarrow K_{\text{diff}} \star \mathbf{S}$.

B. Extension to Multichannel or Vector-Valued Data

Multichannel nonlinear registration algorithms were mostly developed for the registration of DT-MRI [51]–[58]. They were recently applied to the simultaneous fusion of multiple modalities [59] and to the construction of multichannel atlas with different modalities [60]. Among those registration algorithms, an extension of the Demons algorithm to multichannel data has been proposed for DT-MRI registration based on transformation invariant tensor characteristics [53]. Basically, the authors average the update vector field computed independently for each channel. But in this approach, the real coupling between the channels is lost and approximated by averaging the update vector fields. Yeo *et al.* [58] preserved

this coupling by extending the Demons algorithm to vector-valued images and also including the finite-strain differential to take into account the reorientation of diffusion tensors [61]. In our case, we deal with data that do not need any reorientation, but we include a voxel-wise confidence map to each channel. Thus, we can formulate the linearization of the multichannel Demons correspondences energy as follows :

$$E^{\text{corr}}(\mathbf{u}) \simeq \sum_{j=1}^{N} \left(\frac{1}{2|\Omega_j|} \times \int_{\omega \in \Omega_j} \left\| \begin{bmatrix} I_j(\omega) - I'_j \circ S(\omega) \\ \mathbf{0} \end{bmatrix} + \begin{bmatrix} \mathbf{G}_j^T(\omega) \\ \sigma_j(\omega)/\sigma_c \ \text{Id} \end{bmatrix} \mathbf{u}(\omega) \right\|^2 \alpha_j(\omega) \ d\omega \right) \tag{8}$$

where N is the number of channels, Ω_j is the overlap between I_j and I'_j, $\mathbf{G}_j = \frac{1}{2}(\nabla I_j(\omega) + \nabla I'_j \circ S(\omega))$ is the spatial gradient of intensity in channel j whose formulation comes from a linearization of the ESM scheme detailed in [36], σ_j is the local noise estimation in channel j, and $\alpha_j > 0$ the voxel-wise weight map for the channel j.

Its minimization gives the following equation to solve at each voxel :

$$\sum_{j=1}^{N} \alpha_j (\mathbf{G}_j \mathbf{G}_j^T + \sigma_j^2/\sigma_c^2 \ \text{Id}) \ \mathbf{u} = -\sum_{j=1}^{N} \alpha_j (I_j - I'_j \circ S) \ \mathbf{G}_j$$

Considering the eigen decomposition $\sum_{i=1}^{3} \lambda_i^2 \mathbf{e}_i \mathbf{e}_i^T$ of the 3×3 symmetric positive matrix $D = \sum_{j=1}^{N} \alpha_j \mathbf{G}_j \mathbf{G}_j^T$, the update vector field becomes :

$$\mathbf{u} = \sum_{i=1}^{3} \frac{P_i}{\lambda_i^2 + \sigma^2/\sigma_c^2} \ \mathbf{e}_i \tag{9}$$

where $P_i = -\left(\sum_{j=1}^{N} \alpha_j (I_j - I'_j \circ S) \ \mathbf{G}_j^T \right) \mathbf{e}_i$ and $\sigma^2 = \sum_{j=1}^{N} \alpha_j \sigma_j^2$, and σ_c is a parameter that constrains the maximum step length such that the update vector field verifies $\|\mathbf{u}\| \leq \sigma_c \sqrt{d}/2$ (d the number of spatial dimensions in the image). The coupling between channels relies on the eigen decomposition of the sum D of the dyadic tensors $\alpha_j \mathbf{G}_j \mathbf{G}_j^T$. This formulation should improve the speed and accuracy of the convergence compared to previous multichannel approach with Demons algorithm [53], especially in the case of non-aligned gradient vectors.

The *Multichannel Diffeomorphic Demons* (MDD) algorithm is similar to the *Diffeomorphic Demons* (DD) algorithm except that at step (B.1) the update vector field should be computed with Equation 9 instead of Equation 7.

V. Experiments

In order to evaluate the advantages of the proposed registration method based on the multichannel 3D registration with trajectory constraints, we compare it to other methods based on the 3D registration of scalar-valued images with or without the trajectory constraints. When trajectory constraints are considered, the reference frame is set as the ED frame that is the first frame of the 4D cardiac CT sequences. To use these trajectory constraints as mentioned in section III, motion tracking is previously performed in each sequence with an updated Lagrangian scheme where the registration of the current frame k to the reference frame 1 is initialized with the registration result of the previous frame $k-1$ to the reference frame 1. We used the DD algorithm [36] described in Section IV-A for pairwise registration with the following parameters in both synthetic and real data experiments: diffusion-like regularization $\sigma_{\text{diff}} = 1$, maximum update field length bounded with $\sigma_c = 1$, and 30 iterations (stopped if the similarity measure increases) at each of the 3 levels of multiscaling (each dimension size divided by 2 at each level). The resulting motion transformations $M_{1,k}$ and $M'_{1,k}$ are considered as fixed during the estimation of the intersequence transformations S_k. The inversion of motion transformations is also necessary when using trajectory constraints. This inversion is performed by minimizing a functional as described in [62].

The different methods we use to register sequences are the following:

- ***3D direct***: each intersequence transformation S_k is computed independently from the others.
- ***3D sequential***: the computation of the intersequence transformation S_k is initialized with the transformation $M'_{k,k-1} \circ S_{k-1} \circ M_{k,k-1}^{-1}$ using the previously computed transformation corrected with the motion tracking to satisfy the trajectory constraints.
- ***3D + TC***: solely the intersequence transformation S_1 in the ED frame is computed independently from the others that are then reconstructed from S_1 and the motion tracking in both sequences to satisfy the trajectory constraints (TC).
- ***3D average + TC***: solely the intersequence transformation S_1 is computed using the average grey-level image of all the frames registered to the reference ED frame with the motion tracking. The intersequence transformations S_k at other time-points are then reconstructed from S_1 and the motion tracking to satisfy the trajectory constraints (TC).
- ***3D MC + TC***: solely the intersequence transformation S_1 is computed using the multichannel (MC) registration of vector-valued image whose components are all the frames registered to the reference ED frame. The intersequence transformations S_k at other time-points are then reconstructed from S_1 and the motion tracking to satisfy the trajectory constraints (TC). This method corresponds to the 4D spatial registration algorithm presented in Section III in which the multichannel registration is performed with the MDD detailed in Section IV-B.

These methods can be divided into three groups. First, the group of registration methods that perform a 3D scalar-valued image registration at each time point. We call this group the "3D" methods (*3D direct* and *3D sequential*). Second, the group of registration methods that perform a 3D scalar-valued image registration at a reference time-point and that reconstruct the other intersequence transformations using the trajectory constraints. We call this group the "3D + TC" methods (*3D + TC* and *3D average + TC*). And the last group uses the 3D multichannel registration method at a reference time-point and reconstructs the other intersequence transformations using the trajectory constraints. We call this

group the "3D MC + TC" method (*3D MC + TC*). The comparison between the "3D" methods and the two other groups of methods, "3D + TC" and "3D MC + TC" methods, will show the advantage of registering a single reference time-point and using the trajectory constraints to reconstruct the other intersequence transformations. And the comparison between the "3D + TC" methods group and the "3D MC + TC" methods will show the advantage of using a multichannel registration when registering the reference time-point.

When estimating the intersequence transformation S_k with either scalar-valued (DD) or vector-valued (MDD) registration algorithms, the following parameters are used in both synthetic and real data experiments: fluid-like regularization $\sigma_{\text{fluid}} = 0.5$, diffusion-like regularization $\sigma_{\text{diff}} = 0.5$, maximum update field length bounded with $\sigma_c = 1$, and 100 iterations (stopped if the similarity measure increases) at each of the 3 levels of multiscaling (each dimension size divided by 2 at each level).

Since registration is an ill-posed problem, solely checking the intensity matching between the reference image and the transformed target image to compare the different methods is not sufficient. Different mappings can lead to the same similarity measure. Thus we might perfectly match the intensities without recovering the expected deformation field. The best accuracy measurement of a registration algorithm would be to compare the estimated deformation field to the expected deformation field (e.g., gold standard). Generally these ground truth transformations are not available [63] which makes difficult the validation of registration algorithms, especially in the case of intersubject registration. Thus validation of registration algorithms is often limited to partial ground truth information such as segmentations. To overcome the lack of full ground truth information in patient data, we compare the registration methods with synthetic cardiac sequences simulated from a physiologically realistic electromechanical cardiac model [38] in which the ground truth intersequence and intrasequence transformations are known. With real 4D cardiac CT sequences, we compare the registration methods using semi-automatic segmentations of the LV/RV endocardium and epicardium since the underlying ground truth transformations are unknown. But first of all we present a general comparison study on computation times.

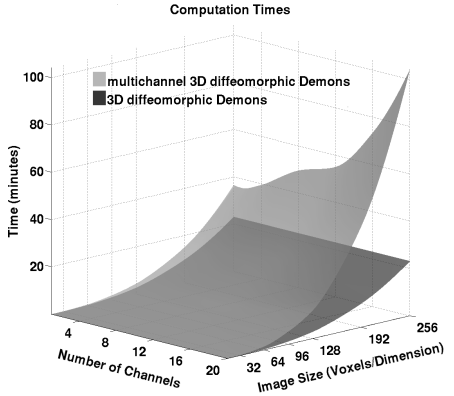

(a) *Diffeomorphic Demons* (DD) vs *Multichannel Diffeomorphic Demons* (MDD) for single pairwise registration.

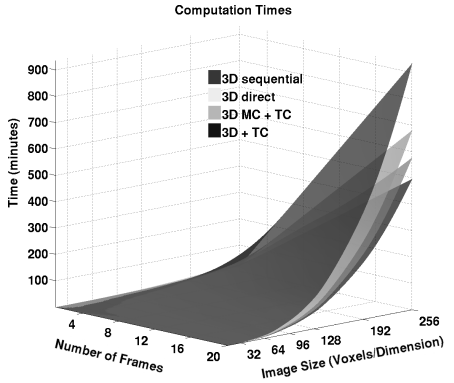

(b) Different registration methods: *3D direct*, *3D sequential*, *3D + TC*, *3D average + TC* (same curve as *3D + TC*), and *3D MC + TC* for registration of two sequences.

Fig. 4. Computation time of different registration algorithms with respect to the number of channels (a) or frames (b), and the size of the images (same size in every dimension X, Y, and Z). The same number of iterations has been performed for each method (30 iterations at each of the 3 levels of multiscaling). Experiments are performed on a PC with Intel Core 2 Duo @ 2.26GHz processor. - (a) Comparison between pairwise registration of scalar-valued images and pairwise registration of vector-valued images. The vector-valued image registration is more time consuming when the number of channels and the size of the image increase significantly. - (b) Comparison between the different methods used to register sequences: *3D direct*, *3D sequential*, *3D + TC* (whose curve is similar as *3D average + TC*), and *3D MC + TC*. The differences between methods increases significantly when the number of frames in the sequence and the size of the images increase.

A. Computation Time Comparison

Computation time is an important issue when dealing with large data as 4D cardiac CT sequences. First, we compare the computation time of the core scalar-valued DD and the vector-valued MDD registration algorithms. Fig. 4 shows that MDD is more time consuming than DD especially when the number of channels and the image size increase significantly. Note that when only one channel is considered, the computation times between the two algorithms are different. Indeed, the MDD is coded with a vectorial data structure that is more complex to handle.

Second, we compare the computation time when registering two sequences with the different methods. In these computation times are included the time to compute the motion tracking in the target sequence used for temporal transformation with motion-based interpolation (all methods), the time to compute the motion tracking in the reference sequence, compose and invert deformation fields when using trajectory constraints (methods with TC and *3D sequential*), the time to compute the intersequence transformations (all methods). Since *3D + TC* and *3D average + TC* have very similar computation times, we only show in Fig. 4 the computation time of *3D + TC*. The results clearly show when estimating the intersequence transformation at every frame takes longer, even if using only 3D scalar-valued registrations that is faster than 3D vector-valued registrations. More registrations are necessary when using the trajectory constraints (additional motion tracking computed in the reference sequence). But since the motion tracking converges faster than intersubject registration (smaller and smoother deformations), the use of

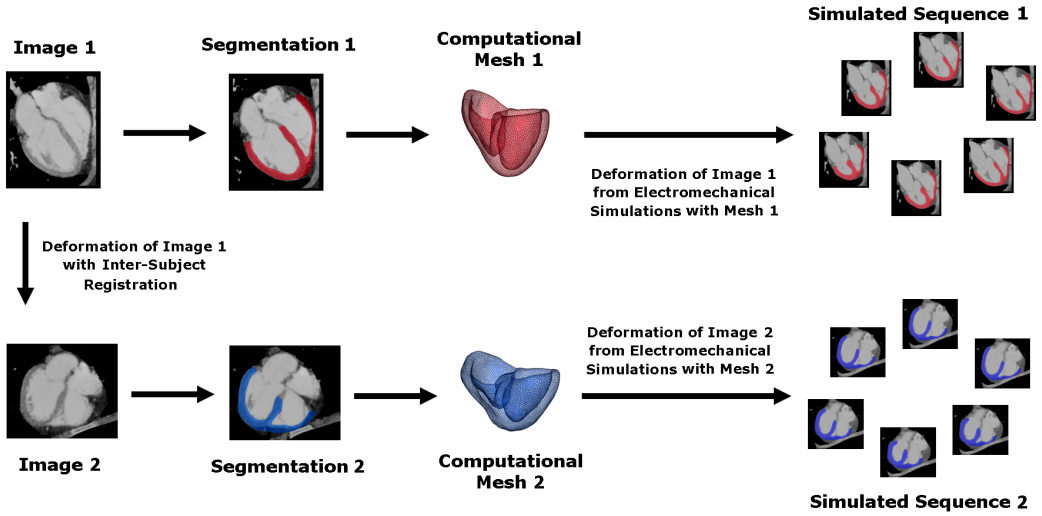

Fig. 5. Construction of simulated sequences using a physiologically realistic electromechanical model of the heart [38]. The ED frame (Image 1) from the 4D cardiac CT sequence of a given patient is segmented (Segmentation 1) to obtain a mesh of the myocardium (Computational Mesh 1). This mesh is used for electromechanical simulations and for creation of a synthetic but physiologically realistic motion of the heart where the deformation fields (extrapolated outside the myocardial mesh) between each frame are known. Based on these deformation fields, the reference image (Image 1) is deformed to create a sequence of images (Simulated Sequence 1). Next the reference ED frame is transformed into the ED frame of another patient (Image 2) with a known deformation field that was computed to best match the anatomy of the two patients. From this image of another anatomy at ED (Image 2), we can apply the same process as previously with Image 1 to build another sequence of images (Simulated Sequence 2). In the end, we obtain two electromechanically simulated sequences whose intrasequence physiological motion transformations and intersequence anatomical transformations are known. These ground truth transformations can be used to assess the accuracy of different registration methods.

trajectory constraints keeps having lower computation times. The *3D sequential* is the most time consuming since trajectory constraints are used and intersequence transformations are estimated at each frame. The *3D MC + TC* method is not the fastest one but has reasonable computation times compared to the fastest *3D + TC* method. The counterpart of the reasonable computation time of the *3D MC + TC* method that solves globally the 4D registration is the memory requirements. Compared to other registration methods that are scalar-valued, the *3D MC + TC* method has memory requirements multiplied by about the number of channels. For instance, in experiments with real data ($174 \times 134 \times 174$ voxels and 20 frames) detailed in the following, a vector-valued registration requires up to about 11 Gb RAM (which can be handled on regular 64 bits PC), whereas a scalar-valued registration requires only up to about 500 Mb RAM.

B. Registration of Electromechanically Simulated Sequences

1) Construction of Electromechanically Simulated Sequences: Previous works [64], [65] already proposed methods to build synthetic 4D cardiac sequences. But these methods do not provide a framework directly applicable to the evaluation of 4D registration in which we need the joint construction of two sequences where both intrasequence and intersequence transformations are fully known. Thus to simulate physiologically realistic and fully controlled time-series of cardiac images, we built two cardiac sequences using an electromechanical model of the heart [38] from a single 4D CT frame as described in Fig. 5.

We start from an initial frame at ED of a real cardiac CT sequence with $190 \times 150 \times 190$ voxels at a resolution of $1.0 \times 1.0 \times 1.0$ mm^3. A segmentation of the myocardium is used as an input for electromechanical simulations of a full cardiac cycle lasting 0.8 seconds. The output of the simulation is a deformation field in the myocardium extrapolated outside the myocardium with an iterative diffusion process. Basically, we perform successive Gaussian smoothing of the deformation field ($\sigma = 1$, 50 iterations) where at each iteration the deformation field in the myocardium is reset to the simulated one and the deformation field farther than 15 mm of the myocardium is reset to be null. Thus, the initial grey-level image at ED can be physiologically deformed to create a sequence over a whole cardiac cycle with a temporal sampling of 20 frames. In the resulting sequence, the ground truth intrasequence motion transformations are known. In order to build a second sequence whose intersequence transformations with the first one are known, we register the initial frame of the first sequence to the anatomy of another real patient. Then, the resulting deformation field is used to transform the initial frame of the first patient and create another cardiac anatomy. Based on this new cardiac anatomy, we simulate another sequence using different parameters chosen such that both sequences have the same cardiac cycle length with corresponding ED and ES physiological time-points. Thus, the two sequences are by construction temporally aligned according to the global physiological events defined for temporal alignment in Section II-B. In this way, we can directly focus on the 4D spatial registration we want to evaluate. Finally, we obtain two electromechanically simulated sequences of 20 frames whose intersequence anatomical and intrasequence motion transformations are fully known. We also created a noisy version of these simulated sequences adding Gaussian noise with different signal-to-noise ratio (SNR ranging from 18 to 54) at each frame.

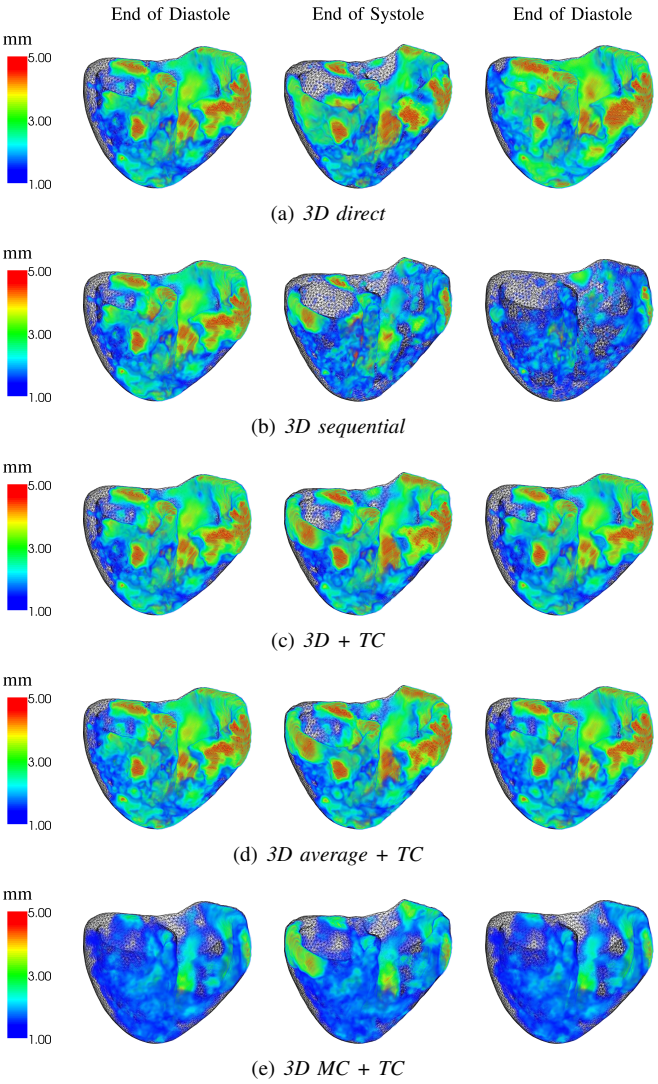

(a) *3D direct*

(b) *3D sequential*

(c) *3D + TC*

(d) *3D average + TC*

(e) *3D MC + TC*

Fig. 6. Registration accuracy with electromechanically simulated sequences - Spatial distribution of differences between the estimated intersequence anatomical transformation S_k and the ground truth transformations in the myocardium of simulated sequences over a cardiac cycle (from ED of current cycle to ED of the next cycle).

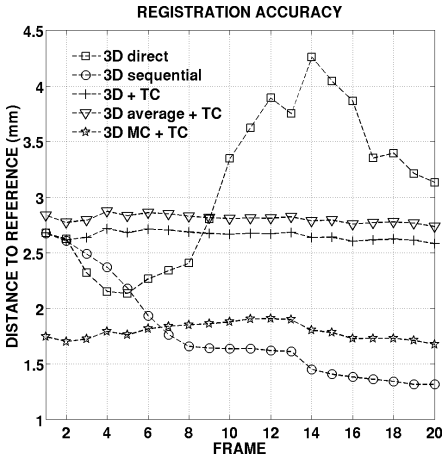

Fig. 7. Registration accuracy with electromechanically simulated sequences - Difference between the computed intersequence anatomical transformations S_k and the ground truth transformations over time in the myocardium.

2) Results: As mentioned previously, since the solution of the registration is not unique (aperture problem), we decided not to use the similarity measure (SSD) as a registration accuracy measure. For the same intensity matching, different transformations are possible. In our experiments, we even noticed that a better matching of the intensities did not necessarily imply a better estimation of the expected ground truth transformation (up to a certain extent). We used two measures to compare the registration algorithms: the distance to the ground truth transformations and the deviation from the trajectory constraints. Both measures are computed solely in a region of interest which is the myocardium.

The distance to the ground truth transformations, which measures the accuracy of the registration at each time-point, is presented in Figs. 6 and 7. The comparison of average motion tracking errors (0.48 mm) and average intersequence registration errors when using trajectory constraints (from 1.79 mm to 2.80 mm) confirms the assumption that motion tracking is more accurately estimated than intersequence transformations and thus can help for the improvement of intersequence registration. The basic *3D direct* registration is not a good strategy with the lowest and most variable registration accuracy over time. The *3D sequential* registration is an improved version of the *3D direct* registration where the intersequence transformations are linked to their temporal neighbors by using the result of the previous time-point registration with motion correction to initialize the registration. The *3D sequential* registration performs the best in terms of registration accuracy after a transient period where *3D MC + TC* registration performs better. Actually, *3D MC + TC* registration is more accurate than other methods performing a single registration at a reference time-point (in our case the ED frame) and reconstructing the spatial transformations at other time-points using the trajectory constraints (*3D + TC* and *3D average + TC*). It shows the advantage of using information from the whole sequence and the advantage of combining this information in a multichannel framework. For instance, the lower registration accuracy of the *3D average + TC* registration shows that the multichannel registration is a good strategy to combine the information from the whole sequence. Averaging the images instead of keeping the original multichannel values yields a blurring of the original information and a loss of structural information. On the other hand the multichannel registration preserves the original intensity values of each frame in a vector. Only the update vector field as formulated in Equation 9 is combining the information from all channels without modifying the original information used for the registration.

Furthermore, the registration methods using the trajectory constraints ("3D + TC" and "3D MC + TC" groups) have more consistent registration accuracy over time than methods of the "3D" group. Trajectory constraints act as a temporal regularization of intersequence transformations. The good results of the *3D MC + TC* registration show that taking into account the information from the whole sequences even in a

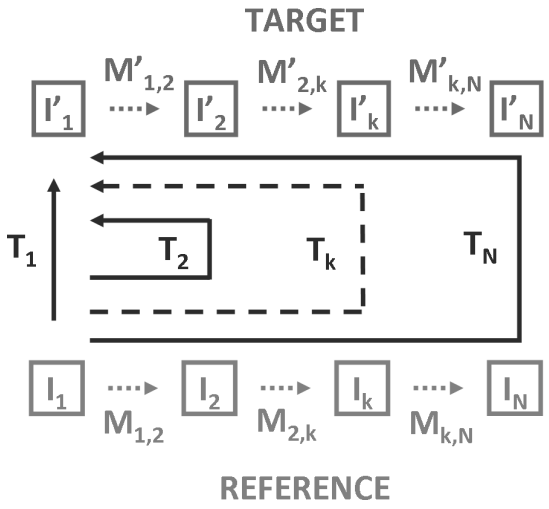

Fig. 8. Deviation from trajectory constraints - The deviation from trajectory constraints is measured by computing the distance between the transformations $T_k = M'^{-1}_{1,k} \circ S_k \circ M_{1,k}$ that should be the same if they satisfy the trajectory constraints. For electromechanically simulated data, we compute it in the whole myocardium. For real data since the accuracy of the registration is restricted to the LV/RV endocardial and epicardial surfaces, we also limit the measure of the deviation to trajectory constraints on these surfaces.

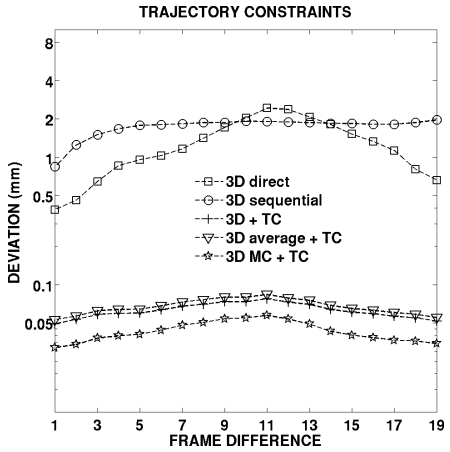

Fig. 9. Trajectory constraints with electromechanically simulated sequences - The deviation from the trajectory constraints in the myocardium is computed by measuring the distance between the transformations T_k corresponding to a given pathway using the intersequence transformation S_k as described in Fig. 8. A log-scale is used for a better visualization of the methods that by construction satisfy the trajectory constraints (*3D + TC*, *3D average + TC*, and *3D MC + TC*). The other methods are significantly less consistent with the motion tracking.

single 3D registration at a given time-point helps to improve the registration accuracy.

The deviation to the trajectory constraints measures the consistency between the intersequence anatomical transformations and the intrasequence motion transformations. This measure of consistency is computed as described in Fig. 8. We perform a pairwise comparison of all the transformations $T_k = M'^{-1}_{1,k} \circ S_k \circ M_{1,k}$ matching the initial reference frames of the two sequences and obtained through different pathways. This measure is complementary to the registration accuracy and different from the registration consistency in loops presented in [27], [28]. A better estimation of the intersequence

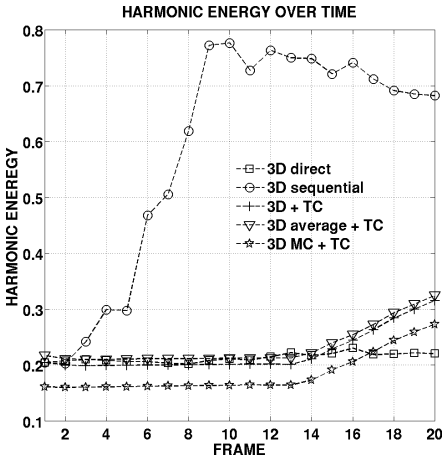

Fig. 10. Harmonic energy with electromechanically simulated sequences - The harmonic energy quantifies the amount deformation in the transformation. The *3D MC + TC* registration gives a much smoother deformation field at the initial reference frame where the multichannel registration is computed.

METHOD	μ_{dist}	σ_{dist}	d_{TC}	HE
3D direct	3.08 mm	1.90 mm	1.27 mm	0.21
3D sequential	1.78 mm	1.33 mm	1.76 mm	0.59
3D + TC	2.65 mm	1.93 mm	0.06 mm	0.22
3D average + TC	2.80 mm	1.92 mm	0.07 mm	0.23
3D MC + TC	1.79 mm	0.97 mm	0.04 mm	0.18

Fig. 11. Results summary of the registration of electromechanically simulated sequences (in myocardium) where μ_{dist} is the distance to ground truth transformations, σ_{dist} is the standard deviation of the distance to ground truth transformations, d_{TC} is the deviation from trajectory constraints, and HE is the harmonic energy.

transformations does not necessarily mean that the deviations to the trajectory constraints get lower, since these deviations are computed with an estimation of the apparent motion, and not the ground truth motion we are not supposed to have access to. In Fig. 9, results show that trajectory constraints are not properly satisfied when computing independently the intersequence transformations at each time-point ("3D" group). In the "3D + TC" and "3D MC + TC" groups, the deviation to trajectory constraints is very low. It was expected since by construction these methods satisfy the trajectory constraints. Actually these errors we observe correspond to residual errors due to composition and inversion of transformations in the reconstruction process. It is important to see that these errors are very low compared to the deviations observed in the "3D" group. It shows that these higher deviations are not due to computational errors when determining the transformations T_k but are mostly due to low consistency between intersequence and intrasequence transformations.

We also measure the smoothness of the intersequence transformation with the harmonic energy of their corresponding deformation fields (the average norm of the Jacobian). As shown in Fig. 10, the harmonic energy are almost the same for every method except the *3D sequential* whose smoothness decreases when registration accuracy increases. Thus the *3D MC + TC* seems to be a good compromise between registration accuracy and smoothness of the resulting deformation field.

Fig. 11 summarizes the performances of each registra-

tion method in terms of registration accuracy, deviation to trajectory constraints, and harmonic energy. Similar results were obtained with noisy simulated sequences except that the registration accuracy with every method dropped in the same proportion compared to noise-free simulated sequences. All these results support the thesis that the *3D MC + TC* registration is the best compromise between accuracy, spatial smoothness, and temporal consistency with motion tracking. But even if these results are obtained with physiologically realistic simulated sequences, the different registration methods still need to be evaluated on experiments with real patient data as in the following.

C. Registration of Real Sequences

1) Data and Processing: In the following experiments, we used 4D cardiac CT sequences acquired with contrast agent at a spatial resolution of about $0.825 \times 0.825 \times 1.00$ mm^3 with $256 \times 256 \times 231$ voxels on 5 different patients with pulmonary stenosis. Since the field of view (FOV) of each acquisition is different, the sequences were cropped to get similar structures in the surrounding area of the heart. The images are then resampled at a spatial resolution of $1.00 \times 1.00 \times 1.00$ mm^3 with $174 \times 134 \times 174$ voxels. The temporal acquisition is synchronized to the ECG from ED over a cardiac cycle with 20 frames. At this temporal resolution, each frame correspond to an acquisition after 5% of R-R time interval (interval between two consecutive R peaks of the ECG).

Since sequences were acquired with contrast agent, we can easily differentiate the blood pool that has higher intensity values than the myocardium. Unfortunately the SSD similarity criterion for registration is meaningless in the blood pool where the intensity values are highly variable in space and time. Since these artifacts can mislead the registration, we first decrease the range of intensity values of the blood pool by linearly transforming the part of the image histogram (basically the intensities higher than a given threshold). Furthermore there might also be intersequence differences in the intensity histogram (for instance a sequence of our dataset had obviously higher intensity values for the myocardium). To avoid a mismatch of corresponding structures using the SSD similarity criterion, we perform a matching of the intensity histogram (*HistogramMatchingImageFilter* from ITK Software Library [66]) between each corresponding frames of the reference and target sequences. The histogram matching is only performed for intersequence registration and not when performing the motion tracking between frames of the same sequence whose intensity histogram are stable over time.

Given the standardized acquisition process of 4D cardiac CT sequences, the global linear temporal registration between different sequences to match the R-R interval is intrinsically performed. The nonlinear part of the temporal transformation is based on blood volume curves (basically obtained with an intensity threshold followed by a main connected component extraction and a closing) that defines a global mechanical state of the heart. Fig. 12 shows the normalized volume curves of each sequence before and after alignment. The temporal transformation is obtained with a Piecewise Cubic Hermite

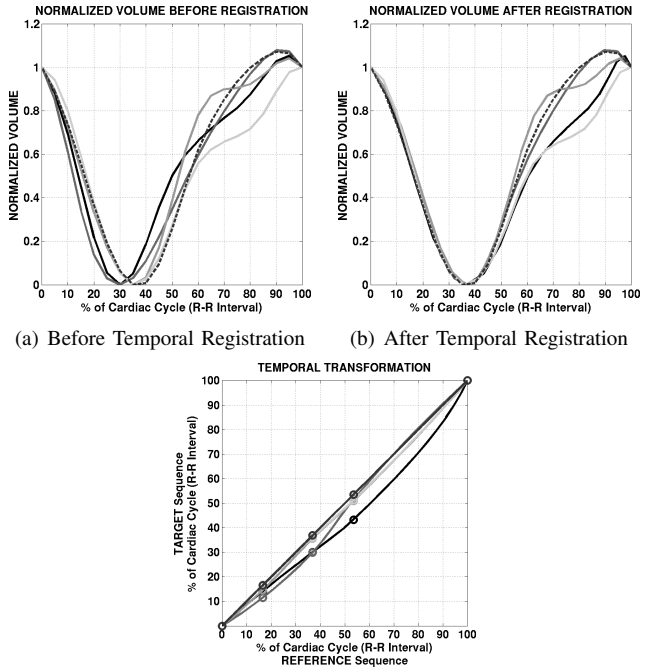

(a) Before Temporal Registration (b) After Temporal Registration

(c) Temporal Transformations

Fig. 12. Normalized blood volume curves (a) before and (b) after temporal registration in each sequence. The dashed black curve is the reference sequence. The continuous curves are the target sequences. The temporal transformations are shown in figure (c).

Interpolating Polynomial (PCHIP) matching specific points of the curves: the first and last frames that corresponds to the linear matching of the R-R interval, the null first derivative of the curve that corresponds to ES, and two null second derivatives of the curves. The resulting transformations have been compared to transformations obtained from ground truth segmentations used in the following to measure the accuracy of 4D registration. Results showed that the error on the temporal transformation was significantly below the temporal resolution of 1 frame: an average of 0.26 frame, a standard deviation of 0.19 frame, and a maximum error of 0.59 frame. It shows that the basic segmentation we proposed is sufficient for the estimation of the temporal transformation. The result of the temporal alignment is shown in Fig. 12. Once the temporal transformation is known, the target sequence is temporally resampled using a motion-based interpolation [1], as well as its corresponding intrasequence motion transformations.

For 4D spatial registration, we first choose the reference frame as the ED frame (first initial frame in each sequence that correspond to the acquisition at the R peak of the ECG). This reference frame is used to perform motion tracking with an updated Lagrangian scheme that provides a temporal causality : estimation of the motion transformations $M_{1,k}$ registering a given frame at a time-point t_k to the reference frame at the reference time-point t_1 with an initial transformation set as the motion transformation $M_{1,k-1}$. Then a reference sequence is chosen among the dataset on which the other ones are registered using the methods presented at the beginning of section V. The intersequence registrations are initialized with an affine transformation determined by matching the blood

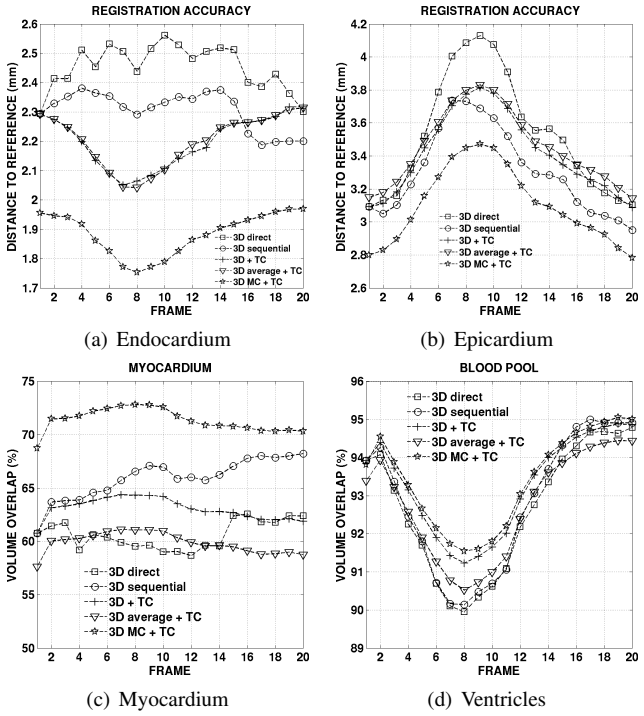

(a) Endocardium (b) Epicardium

(c) Myocardium (d) Ventricles

Fig. 13. Registration accuracy with real sequences - We measure the accuracy of the registration by computing a symmetric distance between the reference and transformed LV/RV endocardial (a) and epicardial (b) surface meshes. We also measure the accuracy of the registration by computing the volume overlap of the myocardium (c) and ventricles (d) between the reference sequence and the transformed target sequence. The improvement of the volume overlap of the ventricles is low by using *3D TC + MC* method. And the volume overlap of the myocardium is significantly improved. All registration accuracy measures are an average over all the patients.

volumes previously determined for temporal alignment.

2) Results: Since we do not have access to the ground truth transformations, we rely on a partial ground truth information, the segmentations of the myocardium with a semi-automatic delineation of the LV/RV endocardium and epicardium. Thanks to the image quality and the high contrast of intensities between the myocardium and the blood pool, the endocardium is easily identified in the sequences. We performed a supervised segmentation of the endocardium in the reference frame (ED) using a single connected-component surface isovalue that has been interactively restricted to be below the valve plane and visually checked. On the other hand, the epicardium is difficult to define solely in terms of intensity features due to the low intensity gradient between the heart and neighboring organs in some areas. The segmentation of the epicardium is performed interactively by manually adding landmarks that lie on the epicardial surface interpolated with radial basis functions. These segmentations in the reference frame are then propagated over the whole sequence with motion transformations.

To measure the accuracy of the registration, we first compute in each frame a symmetric distance between the reference surface transformed with S_k and the target surfaces. Results show that the *3D MC + TC* registration performs better than others (see Figs. 14, 13, and 18) with an improvement of about 11% compared to the second best method and about 17% compared to the *3D direct* method. For every method, registration accuracy is locally lower in areas where structures are more complex and where there is low intensity gradient between neighboring organs for the epicardium. To cope with this low intensity gradient, an additional information is necessary to guide the registration. For instance, one could think about segmenting organs surrounding the myocardium before registration and use it to constrain the registration. For instance, the RV apex is a narrow region where the complex structures of trabeculæ that are highly variable between patients make the registration more difficult. The *3D sequential* registration does not perform as well with real data as with electromechanically simulated data but still improves the *3D direct* method. It probably shows some limitations of simulated data which are not as complex as real data. For instance, both simulated sequences were built from the same reference intensity image making the registration task easier. For real data, we observe that the group of "3D" methods are clearly not as good as the others. It shows the limitations of the 3D pairwise registration of scalar-valued images for large intersubject deformations, especially when getting closer to the ES frame. When using the information from the motion tracking, which is easier to obtain with more accuracy than intersubject anatomical registration, the registration is more consistent over time. The use of the trajectory constraints acts as a temporal regularization of the intersequence transformations with a stronger and more realistic *a priori* regularization between intersequence transformations than a basic smoothing that could not handle high motion speed and acceleration between frames. We also computed the volume overlap of the ventricles and the myocardium between the reference and transformed target sequences [30] to evaluate the registration accuracy as shown in Fig. 13. These volume overlaps are improved when using motion tracking information and even more when using multichannel registration.

As described in Fig. 8, the deviation to trajectory constraints is measured comparing the reference endocardial surface deformed with the transformations $T_k = M'^{-1}_{1,k} \circ S_k \circ M_{1,k}$. The transformation T_k corresponds to the pathway from ED of the reference sequence to ED of the target sequence using the intersequence transformation S_k. When trajectory constraints are satisfied, all transformations T_k should be the same and thus all transformed endocardial surfaces should match. The deviation to trajectory constraints quantifies the consistency between motion and intersequence transformations. The use of trajectory constraints in the registration process clearly shows the improvement compared to methods computing independently the intersequence transformations at each frame (see Figs. 15 and 16). In this way, the trajectory constraints act as a temporal regularization of the intersequence transformations. This advantage is particularly significant in areas of high curvature of the structures (e.g. the right ventricular apex). As mentioned previously, this high curvature can explain the locally lower registration accuracy but mostly the temporal change of this curvature due to cardiac motion can explain the discrepancies of registration accuracy over time.

To measure the quality of the registration, we also compared the spatial smoothness of the resulting deformation fields. To

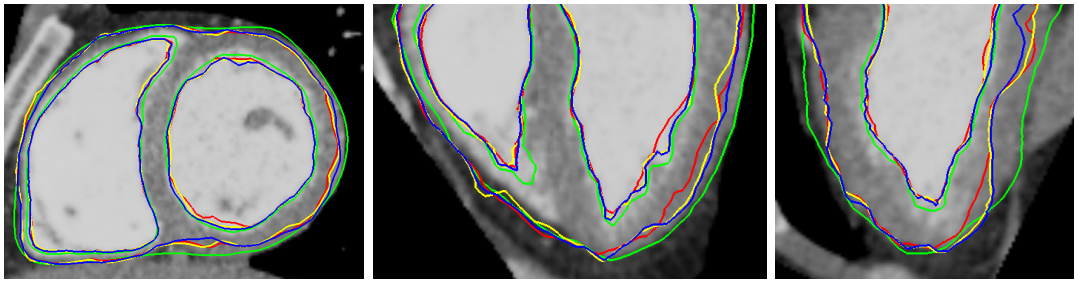

Fig. 14. Registration accuracy with real sequences - We illustrate the accuracy of the registration by showing the transformed LV/RV endocardial and epicardial surfaces with the transformation fields computed with different methods. We only show one method for each group for a better visualization of the differences. The color codes are: *3D direct* in red, *3D + TC* in yellow, *3D MC + TC* in blue, and the ground truth in green. The differences are not apparent everywhere but the *3D MC + TC* provides an overall better registration. Lower registration accuracy appears in areas where structures have high curvature for the endocardium and in areas where there is a low intensity gradient between the heart and neighboring organs for epicardium.

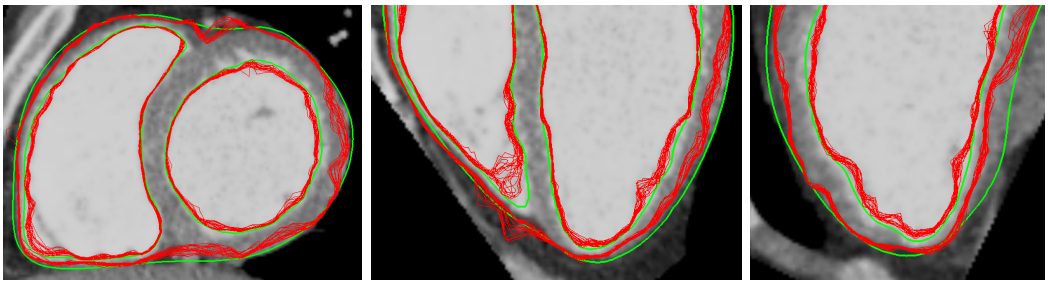

(a) Without trajectory constraints (*3D direct*)

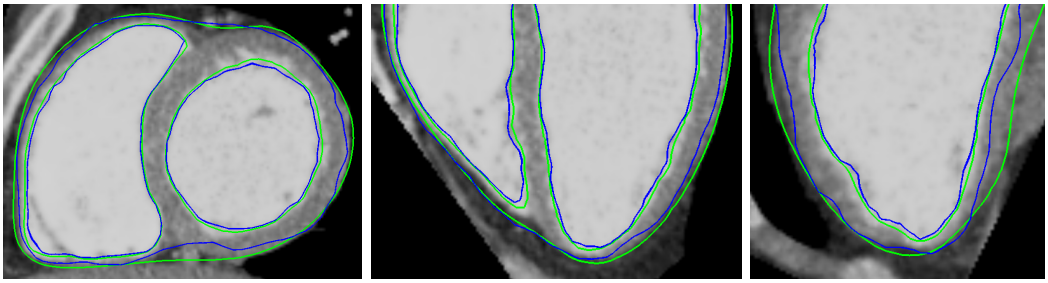

(b) With trajectory constraints (*3D MC + TC*)

Fig. 15. Trajectory constraints with real sequences - We illustrate the deviation from the trajectory constraints with the transformation of the LV/RV endocardial and epicardial surfaces through different pathways in case of *3D direct* registration (first row in red) and in case of *3D MC + TC* registration (second row in blue). The ground truth segmentations are shown in green. When trajectory constraints are satisfied all the transformed contours should perfectly overlay to form a single contour. When the trajectory constraints are not used in the registration process (first row), it is obvious that the transformed contours have high discrepancies showing that the intersequence transformations are not consistent with the motion tracking. On the other hand, when trajectory constraints are used in the registration process (second row), we barely see the differences between transformed contours. The trajectory constraints are satisfied by construction as expected in theory. But it also shows that in practice numerical errors from composition and inversions of transformations are not significant. Showing the ground truth contour in green, we can visualize at the same time the quality of the registration. When trajectory constraints are not used, high discrepancies in quality of registration show that the quality of registration is not consistent over time.

quantify the smoothness of the resulting deformation field, we compute at each time-point their harmonic energy. The lowest is the harmonic energy, the smoothest is the deformation field and the more likely it is to be a realistic solution. As shown in Fig. 17, the *3D MC + TC* method provides the smoothest transformations. Combining the information coming from different time-points directly on the update vector field as formulated in Equation 9 provides intrinsically a smoother deformation field. On the contrary, when using trajectory constraints with 3D scalar-valued registration ("3D + TC" group), the resulting deformation fields are sharper than the "3D" group.

In terms of computation times, different methods have pretty similar computation times except for the *3D sequential* method that is slower than others (cf. Fig. 18). In addition to temporal alignment (mostly motion tracking in target sequence) and spatial registration (scalar-valued or vector-valued), computation times also take into account the time for motion tracking in reference sequence, inversion and reconstruction of intersequence transformations with trajectory constraints when necessary. The advantage of using the trajectory constraints is that motion tracking is already available for the reference sequence if willing to compare motion between the two sequences.

Finally, results with real data also support the thesis that the *3D MC + TC* method is a good compromise between registration accuracy, temporal consistency with motion tracking,

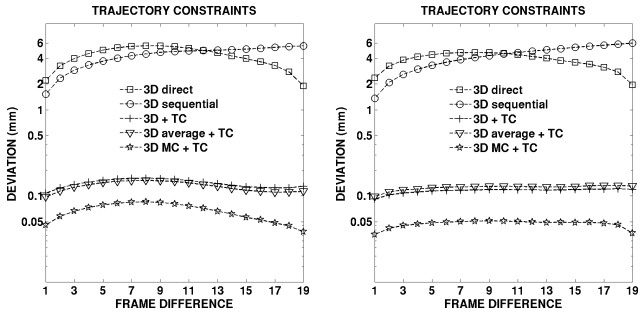

(a) Endocardium (b) Epicardium

Fig. 16. Trajectory constraints with real sequences - The deviation from the trajectory constraints is computed with a distance between transformed segmentations through different pathways as shown in Fig. 8. We compare all the transformed segmentations to each other. We plot this deviation with respect to the distance in frames between the two intersequence transformations used by a given pathway. A log-scale is used for a better visualization of the methods that by construction satisfy the trajectory constraints (*3D + TC*, *3D average + TC*, and *3D MC + TC*). The other methods are less consistent with the motion tracking as also shown in Fig. 15 with the transformed segmentations.

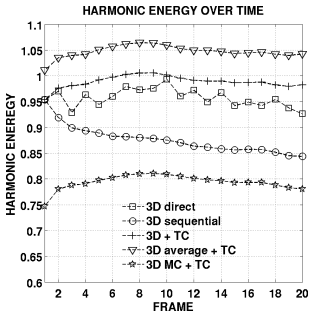

Fig. 17. Harmonic energy with real sequences - The harmonic energy quantifies the amount of deformation in the transformation. A method that gives similar accuracy results with a smoother transformation are more likely to be realistic. The *3D MC + TC* registration provides the smoothest transformation. Whereas the *3D + TC* and *3D average + TC* do not improve and even increase the harmonic energy compared to *3D direct* or *3D sequential* methods.

METHOD	VO	d_{TC}	HE	Time
3D direct	60.6 %	3.82 mm	0.96	56 min
3D sequential	65.9 %	4.07 mm	0.88	86 min
3D + TC	63.1 %	0.12 mm	0.99	47 min
3D average + TC	59.9 %	0.12 mm	1.05	49 min
3D MC + TC	71.3 %	0.05 mm	0.79	59 min

(a) Myocardium

METHOD	μ_{dist}	σ_{dist}	d_{TC}
3D direct	2.45 mm	1.79 mm	4.03 mm
3D sequential	2.31 mm	1.57 mm	4.12 mm
3D + TC	2.20 mm	1.55 mm	0.13 mm
3D average + TC	2.20 mm	1.56 mm	0.12 mm
3D MC + TC	1.88 mm	1.33 mm	0.06 mm

(b) Endocardium

METHOD	μ_{dist}	σ_{dist}	d_{TC}
3D direct	3.52 mm	2.36 mm	3.60 mm
3D sequential	3.30 mm	2.16 mm	4.02 mm
3D + TC	3.41 mm	2.27 mm	0.11 mm
3D average + TC	3.46 mm	2.34 mm	0.12 mm
3D MC + TC	3.10 mm	2.08 mm	0.04 mm

(c) Epicardium

Fig. 18. Results summary of the registration of real sequences where μ_{dist} is the distance to ground truth transformations, σ_{dist} is the standard deviation of the distance to ground truth transformations, d_{TC} is the deviation from trajectory constraints, HE is the harmonic energy, VO is the volume overlap, and Time is the computation time. Computation times were performed with a PC with an AMD Opteron 246 @ 2GHz processor with 12Gb RAM. In these computation times are taken into account the time to perform the intersequence registration, to compute motion tracking, to align temporally the sequences, and to reconstruct of transformations with trajectory constraints when necessary.

spatial smoothness, and computation time.

D. Ventricular Remodeling Analysis after Therapy

We present here an example of potential clinical application where 4D spatiotemporal registration could help in analyzing the remodeling process of the heart after therapy. Pre- and post-operative sequences are compared in case of atrial fibrillation (AF) before radiofrequency ablation (RFA) and 3 months after. AF is the most common sustained cardiac arrhythmia where electrical impulses from sinoatrial nodes are overwhelmed by disorganized electrical impulses coming from the atria and pulmonary veins. The conduction of irregular impulses to the ventricles affects the rhythm of ventricular contraction and thus the cardiac mechanical function. It leads to hypertension, left atrial enlargement, and left ventricular hypertrophy. In case of hypertrophy, the contraction is faster and more powerful to cope with the increase of pressure but it has a limited range of motion with a difficulty to relax properly. RFA is a common intervention for AF where the correction of the electrical activity in the left atrium is related to the regression of left ventricular hypertrophy [67].

Common indices of cardiac function are not always sufficient to explain remodeling processes of the heart after therapy. We propose to use the 4D spatiotemporal registration framework to refine the analysis of the regression of left ventricular hypertrophy after therapy and its impact on cardiac function.

We used two 4D cardiac CT sequences acquired with contrast agent at different spatial and temporal resolutions. The pre-operative sequence is acquired at a spatial resolution of $0.51 \times 0.51 \times 1.00$ mm^3 with $512 \times 512 \times 249$ voxels and a temporal resolution of 10 frames for a cardiac cycle. The post-operative sequence is acquired at a spatial resolution of $0.88 \times 0.88 \times 1.00$ mm^3 with $256 \times 256 \times 182$ voxels and a temporal resolution of 20 frames for a cardiac cycle. Both sequences are resampled at a spatial resolution of $1.00 \times 1.00 \times 1.00$ mm^3 with $226 \times 226 \times 182$ voxels and a temporal resolution of 10 frames for a cardiac cycle.

The post-operative sequence is spatiotemporally registered to the pre-operative sequence under trajectory constraints with MDD as described in Section V-C. First of all, the temporal transformation (computed from the ECG and the blood volume curves) shows a lengthening of the systolic phase from 20% of R-R interval before therapy to a more standard value of 35% after therapy (cf. Fig. 19). Then we estimate the intersequence transformation at each frame of the cardiac cycle that matches cardiac anatomies at corresponding physiological states. As one of the possible measurement of the impact of anatomical

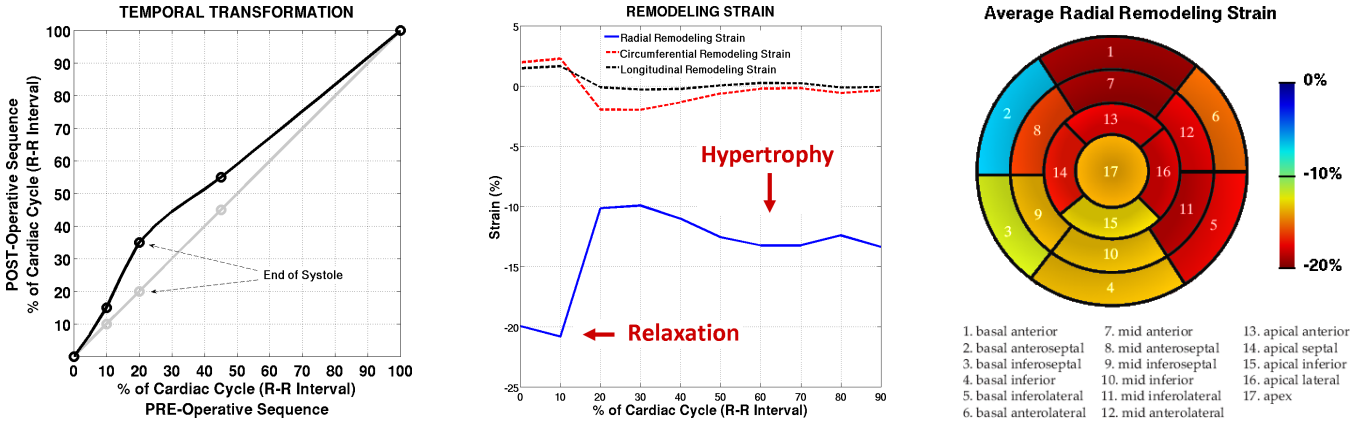

(a) Temporal transformation

(b) Remodeling strains over a cardiac cycle of pre-operative sequence

(c) Average radial remodeling strain over a cardiac cycle (bull's eye view)

Fig. 19. (a) Temporal transformation between pre- and post-operative sequences showing a modification of cardiac dynamic with a lengthening of systolic phase after therapy. - (b) Remodeling strains in radial, circumferential, and longitudinal directions of the prolate coordinate system over a cardiac cycle with temporal alignment of the sequences. Negative strain values mean that contraction occurs after therapy (for instance wall thickness decreases after intervention when radial strain is negative). - (c) Average radial remodeling strain over a cardiac cycle in AHA zones showing regional wall thickness differences due to hypertrophy of left ventricular myocardium.

remodeling on the LV function, we propose to analyze these transformations between pre- and post-operative sequences. We introduce here the new concept of *remodeling strain* defined as the Lagrangian finite strain tensor R_k is computed from the intersequence transformations $S_k = \mathrm{Id} + \mathbf{S}_k$:

$$R_k = 1/2\ (\nabla \mathbf{S}_k + \nabla \mathbf{S}_k^\top + \nabla \mathbf{S}_k^\top \nabla \mathbf{S}_k)$$

The projection of this strain tensor in the prolate coordinate system provides the radial, circumferential and longitudinal remodeling strains (respectively R_k^{rad}, R_k^{circ} and R_k^{long}) at each frame. The radial remodeling strain can be interpreted as intersequence wall thickness change that for instance occurs in case of hypertrophy. Negative radial remodeling strain means a decrease of wall thickness.

As shown in Fig. 19, the average radial remodeling strain between pre- and post-operative sequences is about -12% showing the anatomical remodeling effect of RFA with a global regression of hypertrophy. The temporal variation of radial remodeling strain over the cardiac cycle shows that intersequence wall thickness change is more important at ED than at ES. This higher radial remodeling strain at ED (about -20%) can be explained by the combination of two phenomena: the regression of hypertrophy (anatomical remodeling) and the improvement of the relaxation stage during diastole (functional remodeling). A bull's eye view of the average regional radial strain in each AHA zone presented in Fig. 19 shows a higher regression of left ventricular hypertrophy in the anterior and lateral zones.

This example shows the potential of 4D spatiotemporal registration to analyze the impact of therapy on cardiac anatomy and function by estimating the intersequence transformations over time. Further studies on remodeling strains with larger databases would help to better understand the anatomical and functional impact of remodeling processes.

VI. Conclusion and Perspectives

The spatiotemporal registration of different 4D sequences (or any time-series images such as longitudinal studies) is a complex registration problem whose solution should match corresponding time-points and trajectories of physical points. In this article, we presented a "divide and conquer" method that first decouples the 4D temporal and spatial registrations. The temporal transformation is defined as matching corresponding physiological states and the spatial transformation is defined as matching corresponding anatomical points at each corresponding time-point preserving the homology between points over time. Second, this "divide and conquer" method decomposes the 4D spatial registration problem into a single 3D intersequence anatomical registration and intrasequence motion tracking. First, the newly proposed method has better accuracy than other standard methods. Our registration algorithm showed to be a good solution to solve the 3D intersubject registration by properly combining information from the whole sequence to obtain a more accurate registration and smoother spatial regularization at the same time. Second, it satisfies by construction the trajectory constraints and thus preserves the homology between physical points over time. The use of the trajectory constraints can be seen as a temporal regularization consistent with the motion occurring in each sequence as opposed to standard regularization methods (for instance, B-Spline or Gaussian smoothing).

Since in this framework the temporal transformation is not solely image-driven (e.g. using electrophysiology like the ECG), we stated that the temporal transformation matching corresponding physiological events could be determined independently from the spatial transformations. Purely image-driven joint spatial and temporal registrations could also have been considered. But as shown in Perperidis *et al.* [30], this joint registration increases a lot the computation time. Moreover, the interpretation of the temporal transformation in terms of physiological events is not apparent. But on the other

hand, joint spatial and temporal registrations could still be useful when no physiological event has been clearly identified for temporal registration.

This framework also rely on the estimation of the motion transformations used with the trajectory constraints to simplify the registration. Any improvement of the motion tracking algorithm, for instance by including biomechanical constraints such as near incompressibility, would improve the estimation of the intersequence anatomical transformations. Furthermore, we use trajectory constraints as hard-constraints. One could think of relaxing these hard-constraints by including uncertainties of motion tracking.

The 4D registration under trajectory constraints with *Multi-channel Diffeomorphic Demons* showed promising results on both real patient data and synthetic data simulated with a physiologically realistic electromechanical cardiac model. A more thorough validation is still necessary on a larger database of patients and with a specific clinical application. Nevertheless our study already showed the new possibilities offered by the 4D spatiotemporal registration method to compare two time-series of cardiac images of different patients (intersubject comparison of anatomy and function) or of the same patient at different times (intrasubject comparison such as before and after therapy, or at rest and during exercise).

ACKNOWLEDGMENT

This research was partially funded by INRIA (Sophia Antipolis, France), Siemens Corporate Research (Princeton, NJ, USA), and Microsoft Research (Cambridge, UK). We are grateful of Dr Harold Litt from the Hospital of University of Pennsylvania for provision of 4D CT datasets. We thank Xavier Pennec and Tommaso Mansi for very helpful scientific discussions.

REFERENCES

[1] J. Ehrhardt, D. Säring, and H. Handels, "Optical Flow Based Interpolation of Temporal Image Sequences," in *Proceedings of the Society of Photographic Instrumentation Engineers Conference (SPIE'06)*, vol. 6144, no. 2, 2006, p. 61442K.

[2] E. Angelini, A. Laine, S. Takuma, J. Holmes, and S. Homma, "LV Volume Quantification via Spatiotemporal Analysis of Real-Time 3-D Echocardiography," *IEEE Transactions on Medical Imaging*, vol. 20, no. 6, pp. 457–469, 2001.

[3] J. Bosch, S. Mitchell, B. Lelieveldt, F. Nijland, O. Kamp, M. Sonka, and J. Reiber, "Automatic Segmentation of Echocardiographic Sequences by Active Appearance Motion Models," *Magnetic Resonance in Medicine*, vol. 21, no. 11, pp. 1374–1383, 2002.

[4] M. Lorenzo-Valdés, G. Sanchez-Ortiz, A. Elkington, R. Mohiaddin, and D. Rueckert, "Segmentation of 4D Cardiac MR Images Using a Probabilistic Atlas and the EM Algorithm," *Medical Image Analysis*, vol. 8, no. 3, pp. 255–265, 2004.

[5] J. Montagnat and H. Delingette, "4D Deformable Models with Temporal Constraints: Application to 4D Cardiac Image Segmentation," *Medical Image Analysis*, vol. 9, no. 1, pp. 87–100, 2005.

[6] K. D. Fritscher, R. Pilgram, and R. Schubert, "Automatic Cardiac 4D Segmentation Using Level Sets," in *Proceedings of the 3rd International Conference on Functional Imaging and Modeling of the Heart (FIMH'05)*, vol. 3504 of LNCS, 2005, pp. 113–122.

[7] B. Lelieveldt, A. Frangi, S. Mitchell, H. van Assen, S. Ordas, J. Reiber, and M. Sonka, "3D Active Shape and Appearance Models in Cardiac Image Analysis," in *Mathematical Models in Computer Vision: The Handbook*, 2006th ed., F. Paragios, Chen, Ed. Springer, 2006, pp. 471–485.

[8] M. Uzumcu, R. van der Geest, C. Swingen, J. Reiber, and B. Lelieveldt, "Time Continuous Tracking and Segmentation of Cardiovascular MR Images using Multi-Dimensional Dynamic Programming," *Investigative Radiology*, vol. 41, no. 1, pp. 52–62, 2006.

[9] T. Kohlberger, D. Cremers, M. Rousson, R. Ramaraj, and G. Funka-Lea, "4D Shape Priors for a Level Set Segmentation of the Left Myocardium in SPECT Sequences," in *Proceedings of the 9th International Conference on Medical Image Computing and Computer-Assisted Intervention (MICCAI'06)*, vol. 4190 of LNCS, 2006, pp. 92–100.

[10] J. Cousty, L. Najman, M. Couprie, S. Clément-Guinaudeau, T. Goissen, and J. Garot, "Automated, Accurate and Fast Segmentation of 4D Cardiac MR Images," in *Proceedings of the 3rd International Conference on Functional Imaging and Modeling of the Heart (FIMH'05)*, vol. 4466 of LNCS, 2007, pp. 474–483.

[11] R. Casero and J. Noble, "A Novel Explicit 2D+t Cyclic Shape Model Applied to Echocardiography," in *Proceedings of the 11th International Conference on Medical Image Computing and Computer-Assisted Intervention (MICCAI'08)*, vol. 5242 of LNCS, 2008, pp. 527–534.

[12] D. Perperidis, "Spatio-Temporal Registration and Modelling of the Heart using Cardiovascular MR Imaging," Ph.D. dissertation, Imperial College London, 2005.

[13] C. Hoogendoorn, F. Sukno, S. Ordás, and A. Frangi, "Bilinear Models for Spatio-Temporal Point Distribution Analysis," *International Journal of Computer Vision*, pp. 1573–1405, 2009.

[14] J. Prince and E. McVeigh, "Motion Estimation from Tagged MR Image Sequences," *IEEE Transactions on Medical Imaging*, vol. 11, no. 2, pp. 238–249, 1992.

[15] J. Park, D. Metaxas, A. Young, and L. Axel, "Deformable Models with Parameter Functions for Cardiac Motion Analysis from Tagged MRI Data," *IEEE Transactions on Medical Imaging*, vol. 15, no. 3, pp. 278–289, 1996.

[16] J. Declerck, J. Feldmar, and N. Ayache, "Definition of a Four-Dimensional Continuous Planispheric Transformation for the Tracking and the Analysis of Left-Ventricle Motion," *Medical Image Analysis*, vol. 2, no. 2, pp. 197–213, 1998.

[17] N. Osman, W. Kerwin, E. McVeigh, and J. Prince, "Cardiac Motion Tracking Using CINE Harmonic Phase (HARP) Magnetic Resonance Imaging," *Magnetic Resonance in Medicine*, vol. 42, no. 6, pp. 1048–1060, 1999.

[18] J. Huang, D. Abendschein, V. Dvila-Romn, and A. Amini, "Spatio-Temporal Tracking of Myocardial Deformations with a 4-D B-Spline Model from Tagged MRI," *IEEE Transactions on Medical Imaging*, vol. 18, no. 10, pp. 957–972, 1999.

[19] J. McEachen, A. Nehorai, and J. Duncan, "Multiframe Temporal Estimation of Cardiac Nonrigid Motion," *IEEE Transactions on Image Processing*, vol. 9, no. 4, pp. 651–665, 2000.

[20] R. Chandrashekara, R. Mohiaddin, and D. Rueckert, "Analysis of 3-D Myocardial Motion in Tagged MR Images Using Nonrigid Image," *IEEE Transactions on Medical Imaging*, vol. 23, no. 10, pp. 1245–1250, 2004.

[21] M. Ledesma-Carbayo, J. Kybic, M. Desco, A. Santos, M. Sühling, P. Hunziker, and M. Unser, "Spatio-Temporal Nonrigid Registration for Ultrasound Cardiac Motion Estimation," *IEEE Transactions on Medical Imaging*, vol. 24, no. 9, pp. 1113–1126, 2005.

[22] B. Delhay, "Estimation Spatio-temporelle de Mouvement et Suivi de Structures Déformables. Application à l'Imagerie Dynamique du Cœur et du Thorax." Ph.D. dissertation, INSA Lyon, 2006.

[23] H. Sundar, H. Litt, and D. Shen, "Estimating Myocardial Motion by 4D Image Warping," *Pattern Recognition*, vol. 42, no. 11, pp. 2514–2526, 2009.

[24] A. Bistoquet, J. Oshinski, and O. M. Skrinjar, "Left Ventricular Deformation Recovery From Cine MRI Using an Incompressible Model," *IEEE Transactions on Medical Imaging*, vol. 26, no. 9, pp. 1136–1153, 2007.

[25] D. Sarrut, B. Delhay, P. Villard, V. Boldea, M. Beuve, and P. Clarysse, "A Comparison Framework for Breathing Motion Estimation Methods from 4D Imaging," *IEEE Transactions on Medical Imaging*, vol. 26, no. 12, pp. 1636–1648, 2007.

[26] M. De Craene, O. Camara, B. Bijnens, and A. Frangi, "Large Diffeomorphic FFD Registration for Motion and Strain Quantification from 3D-US Sequences," in *Proceedings of Functional Imaging and Modeling of the Heart (FIMH'09)*, ser. LNCS, vol. 5528, 2009, pp. 437–446.

[27] A. Roche, X. Pennec, G. Malandain, and N. Ayache, "Rigid Registration of 3D Ultrasound with MR Images: a New Approach Combining Intensity and Gradient Information," *IEEE Transactions on Medical Imaging*, vol. 20, no. 10, pp. 1038–1049, 2001.

[28] X. Pennec, A. Roche, P. Cathier, and N. Ayache, "Non-Rigid MR/US Registration for Tracking Brain Deformations," in *Multi-Sensor Image Fusion and Its Applications*, ser. Signal Processing and Communications. CRC Press - Taylor and Francis, 2005, vol. 26, ch. 4, pp. 107–143.

[29] M. Singh, A. Basu, and M. Mandal, "Event Dynamics Based Temporal Registration," *IEEE Transactions on Medical Imaging*, vol. 9, no. 5, pp. 1004–1015, 2007.

[30] D. Perperidis, R. Mohiaddin, and D. Rueckert, "Spatio-Temporal Free-Form Registration of Cardiac MR Image Sequences," *Medical Image Analysis*, vol. 9, no. 5, pp. 441–456, 2005.

[31] Y. Caspi and M. Irani, "Spatiotemporal Alignment of Sequences," *IEEE Transactions on Pattern Analysis and Machine Intelligence*, vol. 24, no. 11, pp. 1409–1424, 2002.

[32] X. Huang, N. Hill, J. Ren, G. Guiraudon, D. Boughner, and T. M. Peters, "Dynamic 3D Ultrasound and MR Image Registration of the Beating Heart," in *Proceedings of the 8th International Conference on Medical Image Computing and Computer-Assisted Intervention (MICCAI'05)*, vol. 3750 of LNCS, 2005, pp. 171–178.

[33] W. Zhang, J. Noble, and J. Brady, "Spatio-temporal Registration of Real Time 3D Ultrasound to Cardiovascular MR Sequences," in *Proceedings of the 10th International Conference on Medical Image Computing and Computer-Assisted Intervention (MICCAI'07)*, vol. 4791 of LNCS, 2007, pp. 343–350.

[34] A. Lopez, K. Fritscher, T. Trieb, R. Schubert, and J. Mattes, "3D Inter-Subject Cardiac Registration Using 4D Information," in *Proceedings of the Society of Photographic Instrumentation Engineers Conference (SPIE'08)*, vol. 6914, 2008, p. 691413.

[35] E. Schreibmann, B. Thorndyke, T. Li, J. Wang, and L. Xing, "Four-Dimensional Image Registration for Image-Guided Radiotherapy," *International Journal of Radiation Oncology Biology Physics*, vol. 71, no. 2, pp. 578–586, 2008.

[36] T. Vercauteren, X. Pennec, A. Perchant, and N. Ayache, "Diffeomorphic Demons: Efficient Non-parametric Image Registration," *NeuroImage*, vol. 45, no. 1, pp. 61–72, 2009.

[37] J.-M. Peyrat, H. Delingette, M. Sermesant, X. Pennec, C. Xu, and N. Ayache, "Registration of 4D Time-Series of Cardiac Images with Multichannel Diffeomorphic Demons," in *Proceedings of the 11th International Conference on Medical Image Computing and Computer-Assisted Intervention (MICCAI'08)*, vol. 5242 of LNCS, 2008, pp. 972–979.

[38] M. Sermesant, H. Delingette, and N. Ayache, "An Electromechanical Model of the Heart for Image Analysis and Simulation," *IEEE Transactions in Medical Imaging*, vol. 25, no. 5, pp. 612–625, 2006.

[39] A. Larson, R. White, G. Laub, E. McVeigh, D. Li, and O. Simonetti, "Self-Gated Cardiac Cine MRI," *Magnetic Resonance in Medicine*, vol. 51, no. 1, pp. 93–102, 2004.

[40] D. Richardson, D. Randall, and D. Speck, *Cardiopulmonary System*, 1st ed. Wiley-Blackwell, 1998.

[41] T. Mansi, J.-M. Peyrat, M. Sermesant, H. Delingette, J. Blanc, Y. Boudjemline, and N. Ayache, "Physically-Constrained Diffeomorphic Demons for the Estimation of 3D Myocardium Strain from Cine-MRI," in *Proceedings of Functional Imaging and Modeling of the Heart (FIMH'09)*, ser. LNCS, vol. 5528, 2009, pp. 201–210.

[42] A. Klein, J. Andersson, B. Ardekani, J. Ashburner, B. Avants, M. Chiang, G. Christensen, D. Collins, J. Gee, P. Hellier, J. Song, M. Jenkinson, C. Lepage, D. Rueckert, P. Thompson, T. Vercauteren, R. Woods, J. Mann, and R. Parsey, "Evaluation of 14 Nonlinear Deformation Algorithms Applied to Human Brain MRI Registration," *NeuroImage*, 2009, In Press.

[43] G. Hermosillo, C. Chefd'Hotel, and O. Faugeras, "Variational Methods for Multimodal Image Matching," *International Journal of Computer Vision*, vol. 50, no. 3, pp. 329–343, 2002.

[44] F. Beg, M. Miller, A. Trouvé, and L. Younes, "Computing Large Deformation Metric Mappings via Geodesic Flows of Diffeomorphisms," *International Journal of Computer Vision*, vol. 61, no. 2, pp. 139–157, 2005.

[45] J. Ashburner, "A Fast Diffeomorphic Image Registration Algorithm," *NeuroImage*, vol. 38, no. 1, pp. 95–113, 2007.

[46] M. Hernandez, M. Bossa, and S. Olmos, "Registration of Anatomical Images Using Geodesic Paths of Diffeomorphisms Parameterized with Stationary Vector Fields," in *Proceedings of MMBIA Workshop of the IEEE 11th International Conference on Computer Vision (ICCV'07)*, 2007, pp. 1–8.

[47] S. Marsland and R. McLachlan, "A Hamiltonian Particle Method for Diffeomorphic Image Registration," in *Proceedings of Information Processing in Medical Imaging (IPMI'07)*, vol. 4584 of LNCS, 2007, pp. 396–407.

[48] B. Avants, C. Epstein, M. Grossman, and J. Gee, "Symmetric Diffeomorphic Image Registration with Cross-Correlation: Evaluating Automated Labeling of Elderly and Neurodegenerative Brain," *Medical Image Analysis*, vol. 12, no. 1, pp. 26–41, 2008.

[49] J.-P. Thirion, "Image Matching as a Diffusion Process: an Analogy with Maxwell's Demons," *Medical Image Analysis*, vol. 2, no. 3, pp. 243–260, 1998.

[50] P. Cachier, E. Bardinet, D. Dormont, X. Pennec, and N. Ayache, "Iconic Feature Based Nonrigid Registration: The PASHA Algorithm," *Computer Vision and Image Understanding*, vol. 89, no. 2-3, pp. 272–298, 2003.

[51] J. Ruiz-Alzola, C.-F. Westin, S. K. Warfield, C. Alberola, S. Maier, and R. Kikinis, "Non-Rigid Registration of 3D Tensor Medical Data," *Medical Image Analysis*, vol. 6, no. 2, pp. 143–161, 2002.

[52] G. K. Rohde, S. Pajevic, C. Pierpaoli, and P. J. Basser, "A Comprehensive Approach for Multi-channel Image Registration," in *Proceedings of 2nd International Workshop on Biomedical Image Registration (WBIR'03)*, vol. 2717 of LNCS, 2003, pp. 214–223.

[53] H.-J. Park, M. Kubicki, M. Shenton, A. Guimond, R. McCarley, S. Maier, R. Kikinis, F. Jolesz, and C.-F. Westin, "Spatial Normalization of Diffusion Tensor MRI Using Multiple Channels," *NeuroImage*, vol. 20, no. 4, pp. 1995–2009, 2003.

[54] H. Zhang, P. A. Yushkevich, D. C. Alexander, and J. C. Gee, "Deformable Registration of Diffusion Tensor MR Images with Explicit Orientation Optimization," *Medical Image Analysis*, vol. 10, no. 5, pp. 764–785, 2006.

[55] Y. Cao, M. I. Miller, S. Mori, R. L. Winslow, and L. Younes, "Diffeomorphic Matching of Diffusion Tensor Images," in *Proceedings of the 2006 Conference on Computer Vision and Pattern Recognition Workshop (CVPRW'06)*, 2006, p. 67.

[56] W. Van Hecke, A. Leemans, E. D'Agostino, S. D. Backer, E. Vandervliet, P. Parizel, and J. Sijbers, "Nonrigid Coregistration of Diffusion Tensor Images Using a Viscous Fluid Model and Mutual Information," *IEEE Transactions on Medical Imaging*, vol. 26, no. 11, pp. 1598–1612, 2007.

[57] M.-C. Chiang, A. Leow, A. Klunder, R. Dutton, M. Barysheva, S. Rose, K. McMahon, G. de Zubicaray, A. Toga, and P. Thompson, "Fluid Registration of Diffusion Tensor Images Using Information Theory," *IEEE Transactions on Medical Imaging*, vol. 27, no. 4, pp. 442–456, 2008.

[58] B. Yeo, T. Vercauteren, P. Fillard, J.-M. Peyrat, X. Pennec, P. Golland, N. Ayache, and O. Clatz, "DT-REFinD: Diffusion Tensor Registration with Exact Finite-Strain Differential," *IEEE Transactions on Medical Imaging*, 2009, in press.

[59] B. B. Avants, J. Duda, H. Zhang, and J. C. Gee, "Multivariate Normalization with Symmetric Diffeomorphisms for Multivariate Studies," in *Proceedings of the 10th International Conference on Medical Image Computing and Computer-Assisted Intervention (MICCAI'07)*, vol. 4791 of LNCS, 2007, pp. 359–366.

[60] T. Rohlfing, N. M. Zahr, E. V. Sullivan, and A. Pfefferbaum, "The SRI24 Multichannel Brain Atlas: Construction and Applications," in *Proceedings of the Society of Photographic Instrumentation Engineers Conference (SPIE'08)*, vol. 6914, no. 1, 2008, p. 691409.

[61] D. C. Alexander, C. Pierpaoli, P. J. Basser, and J. C. Gee, "Spatial Transformations of Diffusion Tensor Magnetic Resonance Images," *IEEE Transactions on Medical Imaging*, vol. 20, no. 11, pp. 1131–1139, 2001.

[62] P. Cachier, "Recalage Non Rigide d'Images Médicales Volumiques - Contribution aux Approches Iconiques et Géométriques," Thèse de sciences, École Centrale des Arts et Manufactures, 2002.

[63] T. Mäkelä, P. Clarysse, O. Sipila, N. Pauna, Q. C. Pham, T. Katila, and I. E. Magnin, "A Review of Cardiac Image Registration Methods," *IEEE Transactions on Medical Imaging*, vol. 21, no. 9, pp. 1011–1021, 2002.

[64] W. P. Segars, M. Mahesh, T. J. Beck, E. C. Frey, and B. M. W. Tsui, "Realistic CT Simulation Using the 4D XCAT Phantom," *Medical Physics*, vol. 35, no. 8, pp. 3800–3808, 2008.

[65] R. Haddad, I. Magnin, and P. Clarysse, "A New Fully-Digital Anthropomorphic and Dynamic Thorax/Heart Model," in *Proceedings of the 29th Annual International Conference of the IEEE on Engineering in Medicine and Biology Society (EMBS'07)*, 2007, pp. 5999–6002.

[66] L. Ibanez, W. Schroeder, L. Ng, J. Cates, the Insight Software Consortium, and R. Hamming, "The ITK Software Guide," 2003.

[67] A. Mattioli, S. Bonatti, D. Monopoli, M. Zennaro, and G. Mattioli, "Left Atrial Remodelling after Short Duration Atrial Fibrillation in Hypertrophic Hearts," *Heart*, vol. 91, no. 1, pp. 91–92, 2005.